Disk sources of the Kerr and Tomimatsu-Sato spacetimes: Construction and physical properties

Tomáš Ledvinka[1,*] and Jiří Bičák[1,2,†]

[1]Institute of Theoretical Physics, Faculty of Mathematics and Physics, Charles University in Prague, V Holešovičkách 2, 180 00 Praha 8, Czech Republic

[2]Max Planck Institute for Gravitational Physics (Albert Einstein Institute), Am Mühlenberg 1, Potsdam 14476, Germany

(Received 7 December 2018; published 27 March 2019)

We construct the disk sources matched to the exact vacuum Kerr and to the two classes of Tomimatsu-Sato spacetimes. We analyze two models of the matter forming these disks. At each radius we consider either a rotating massive ring with pressure or two counter-rotating streams of particles in circular geodesic motion. Dragging effects present in such spacetimes lead either to the rotation of rings or the asymmetry between streams. We demonstrate that the model of rotating rings is general enough to describe all axisymmetric stationary disk sources with vanishing radial pressure which satisfy the weak energy condition, and that centrifugal effects present in the disk sources of spacetimes with large angular momentum prevent the construction of highly compact sources made of counter-rotating streams of geodesic particles. We illustrate the radial distribution of the mass inside the disks and the angular velocities of both geodesic streams.

DOI: 10.1103/PhysRevD.99.064046

I. INTRODUCTION

Gravitating disks and their fields are of great intrinsic interest and have important astrophysical applications. In Newtonian theory one can easily build potential-density pairs for axisymmetric disks by using the method of images common in galactic dynamics. A point mass placed at a distance b below the center $\rho = 0$ of a plane $z = 0$ gives a solution of the Laplace equation above the plane. Then, considering the potential obtained by reflecting this $z \geq 0$ potential in $z = 0$, a symmetrical solution both above and below the plane is obtained which is continuous but has a discontinuous normal derivative on $z = 0$. The jump gives a positive surface density on the plane. In galactic dynamics one considers general line distributions of mass along the negative z axis and, employing the device described above, one finds the potential-density pairs for general axially symmetric disks. In the case of static, axisymmetric vacuum spacetimes in general relativity, as Hermann Weyl showed in 1917, exact solutions of the Einstein equations can, in suitable (cylindrical-type) coordinates, be generated from vacuum solutions of the Laplace equation; hence, classical potentials can be used to generate relativistic solutions. In Ref. [1], an infinite number of new static solutions of the Einstein equations were found starting from realistic potentials used to describe flat galaxies, as given by Evans and de Zeeuw [2]. Although these disks are Newtonian at large distances, in their central regions interesting relativistic features arise, such as velocities close to the velocity of light, and large redshifts. In a more mathematical context, a number of exact static axisymmetric (electro) vacuum solutions of the Einstein equations which involve singularities in their central regions can be interpreted as exact external fields of disk sources. In Ref. [3] it was shown that most vacuum static Weyl solutions, including the Curzon and the Darmois-Voorhees-Zipoy solutions can arise as the metrics of counter-rotating relativistic disks. In order that the disks may be seen as being produced by circulating particles one has to consider them as being made of two equal collisionless streams that circulate in opposite directions around the center. In this way one avoids the effect of dragging of inertial frames which is absent in the static metrics.

Because the dragging of inertial frames implies nonlinear fields outside the disks it is very hard to find analytically expressed exact stationary, asymptotically flat solutions of the Einstein equations corresponding to rotating material sources. Remarkably, the Riemann-Hilbert problem (the boundary value problem) for an infinitesimally thin, finite disk of dust particles which rotate rigidly around a common center was formulated and solved (see Refs. [4,5] and references therein). Later it was generalized to the solutions representing counter-rotating streams [6,7] which in one limit go over to the rigidly rotating disk of the preceding case, and in the other limit to the static counter-rotating finite disks described in Ref. [8]. Although these solutions are very valuable, they are special, and it is thus worthy to construct other types of rotating disk sources.

*tomas.ledvinka@mff.cuni.cz
†jiri.bicak@mff.cuni.cz

The method of images cannot be used directly because of nonlinear fields outside the disks due to dragging. However, the method of images described above may be viewed as the *identification* of the surface $z = b$ with the surface $z = -b$. The field remains continuous but the jump of its normal derivatives induces a matter distribution in the disk. We shall describe and illustrate the procedure in detail in the following section and apply it throughout the paper. Hence, if a stationary vacuum solution containing some pathological regions in the central parts is available, one can always "cut the regions off" and end up with a disk source surrounded by a regular spacetime. It is thus worth using a much wider family of vacuum solutions with "sources" in the form of various singularities or other pathologies to obtain spacetimes with idealized but much more realistic sources in the form of shells and disks. In this way one can substantially enlarge the set of spacetimes on which the complicated relation between source and spacetime parameters can be studied. There is an extensive literature on disk sources constructed by this type of method in vacuum spacetimes (see, e.g., Refs. [9–12]), in electrovacuum spacetimes (e.g., Refs. [13,14]; for a review, see Ref. [15]), and in spacetimes representing a disk with a black hole inside (see, e.g., Refs. [16,17]). Those are just casually selected references; other citations can be found therein. For a comprehensive review on self-gravitating relativistic disks, in particular those around black holes, see Ref. [18] and the more recent work by Semerák, Suková and collaborators (Ref. [19] and references therein) on disks and rings around black holes (for example, the superpositions of a Schwarzschild black hole with the inverted Morgan-Morgan counter-rotating thin disks).

In this paper we consider disks without radial pressure as sources of the first three ($\delta = 1, 2, 3$) members of the Tomimatsu-Sato (TS) class of spacetimes. These are asymptotically flat stationary solutions of the Ernst equation given by rational functions in spheroidal coordinates [20,21]. The TS $\delta = 1$ metric is the well-known Kerr solution of Einstein's equations, the only asymptotically flat stationary spacetime which, under a suitable choice of parameters, represents a rotating black hole with all singularities hidden under the event horizon. Very soon after the discovery of the TS solutions, their properties (for $\delta = 2$) were investigated in Ref. [22]. It was shown that the solutions represent a spinning naked singularity with causality-violating regions and when the parameter $q = 0$ (see below) it reduces to the Voorhees solution. The complicated structure of the TS $\delta = 2$ spacetime center led to the general belief that there is no horizon present there, but its location and shape was revealed in 2003 when Kodama and Hikida investigated in depth the global structure of both the Zipoy-Voorhees-Weyl and the $\delta = 2$ TS spacetimes in ref. [23].

The properties of the central strong-field regions of TS spacetimes are also investigated in this paper where we pose questions, such as (i) how strong gravitational field can be created without violating energy conditions, (ii) how much total angular momentum can a disk producing a TS solution possess, or (iii) what prevents us from constructing disk sources which reveal closed-timelike-curve (CTC) regions known to be present in the central parts of these spacetimes. To summarize our main motivations, we are focused on questions of principle, such as (i) whether there are physically plausible matter sources of known vacuum solutions, often containing naked singularities like in the TS case, or (ii) what effects and possible pathologies arise due to very strong gravitational fields described by exact, explicit, and hence quite idealized, general-relativistic models of disks formed by circular counter-rotating streams or rotating rings with tangential pressure.

Although the work on counter-rotating relativistic disks cannot be directly applied to realistic models of galaxies, the counter-rotating disks have become more attractive since the beginning of the 1990s when counter-rotating disk galaxies were first observed [24]. Since then the counter-rotating components were detected in "tens of galaxies along all the Hubble sequence, from elliptical to irregulars" (see Ref. [25] for a review from 2014). For example, among 53 lenticular (S0) galaxies 17 had counter-rotating gas, i.e., 32%, while less than 10% host a significant fraction of counter-rotating stars. In Ref. [26] from 2017 on the formation of S0 galaxies, the authors cited that "the observation of counter-rotation in galaxies is becoming more commonplace...the percentage of S0 galaxies that exhibit counter-rotation is 20–40 per cent." Mergers appear as the prime candidate for the origin of counter-rotation; however, accretion and other mechanisms are also proposed to explain the formation of such systems. Moreover, recently counter-rotating disks arising from the accretion of counter-rotating gas on the surface of a corotating disk have been considered [27]. The authors gave several scenarios of how such situations may arise on a stellar mass scale. On a larger scale they referred to the idea proposed by King and Pringle [28] in which the rapid growth of massive black holes at high redshifts will be compatible with the Eddington limit of their emission if the gas accretion proceeds as a sequence of clouds with varying angular momenta.

In the following section we show how the method of constructing the disk sources by performing identifications of spacetime hypersurfaces works. The metric induced on the identification hypersurface is invariantly expressed in terms of an appropriate tetrad. The tetrad components of the stress-energy tensor of the disk matter are given in terms of the jumps of the extrinsic curvature of the hypersurface and the discontinuities of metric functions (gravitational potentials). The masses and the angular momenta of the disks are expressed using the Komar integrals. By the procedure described one can always find a disk source for a given solution of the Einstein equations. Often, however, the source cannot be constructed from a physically acceptable matter. In Sec. III we thus formulate criteria (like "energy conditions") that guarantee a physically meaningful source.

The most plausible and physically clear sources are those made from counter-rotating streams of incoherent dust moving along circular geodesics. This model is discussed in detail in Sec. IV. In Sec. V we summarize the main properties of Tomimatsu-Sato spacetimes. In Sec. VI, the properties of the disks are analyzed by both analytical and numerical methods and illustrated by a number of figures. Section VI contains four subsections: one on general Tomimatsu-Sato solutions, one on the Kerr solutions (TS solutions with index $\delta = 1$) with a separate discussion of the disks producing extreme Kerr metrics, and two that describe and illustrate the properties of the TS disks producing the TS metrics with $\delta = 2$ and $\delta = 3$, respectively. The main text comes to an end with our conclusions in which the main results of the paper are summarized. The two Appendixes contain a discussion of the static disks and the derivation of the total mass and total angular momentum of the disks from the Komar integral, respectively.

II. STATIONARY AXISYMMETRIC SPACETIME WITH DISK SOURCES

We start from the metric given in Weyl's canonical form in the Weyl-Papapetrou (WP) coordinates $\{t, \phi, \rho, z\}$ (see e.g., Ref. [29]),

$$ds^2 = -e^{2\nu}(dt + A d\phi)^2 + \frac{e^{2\zeta}}{e^{2\nu}}(d\rho^2 + dz^2) + \frac{\rho^2}{e^{2\nu}} d\phi^2, \qquad (1)$$

where the functions ν, ζ, A depend on ρ, z only. We assume that the metric represents a stationary axisymmetric asymptotically flat vacuum solution of the Einstein equations "above" the axisymmetric hypersurface ${}^{+}\Sigma$ parametrically described by

$$z = z(s), \qquad \rho = \rho(s), \qquad \phi, \qquad t, \qquad (2)$$

where s is a "radial" coordinate from the center of the disk for any $t = \text{const}$. The spacetime "below" the surface is then completed assuming the symmetry of all potentials under the reflection

$$t \to t, \qquad \rho \to \rho, \qquad \phi \to \phi, \qquad z \to -z. \qquad (3)$$

This completion also yields the hypersurface ${}^{-}\Sigma$. For spacetimes globally satisfying the symmetry (3), this construction is equivalent to the exclusion of the "central" region between ${}^{-}\Sigma$ and ${}^{+}\Sigma$; see Fig. 1 which illustrates the identification (coordinates t and ϕ being suppressed).

The hypersurface ${}^{+}\Sigma$ has unit normals given by the following spacetime components:

$$n^\mu = \lambda(s)\left(\rho'(s)\delta^\mu_z - z'(s)\delta^\mu_\rho\right), \qquad (4)$$

$$\lambda(s) = \frac{e^{\nu-\zeta}}{\sqrt{\rho'(s)^2 + z'(s)^2}}. \qquad (5)$$

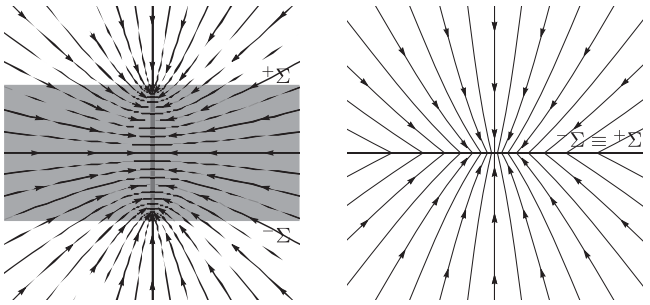

FIG. 1. When the central region between ${}^{-}\Sigma$ and ${}^{+}\Sigma$ (left, shaded) containing an arbitrary source of the field is removed, we obtain the field of a disk source (right).

We use the following convention for indices: $k, l, m, \ldots, \kappa, \lambda, \mu, \ldots = 0, .., 3$, $a, b, c, \ldots, \alpha, \beta, \gamma, \ldots = 0, 1, 2$, $A, B, \ldots = 0, 1$. If the coordinates $x^\mu = \{t, \rho, \phi, z\}$ are used as indices they always mean the particular component ($x^3 \equiv x^z = z$), or the partial derivative with respect to a particular coordinate ($g_{ab,z} = \partial g_{ab}/\partial z$). Tetrad (projected) components of tensors use brackets [see, e.g., Eq. (8)]. An induced metric on the three-dimensional hypersurface ${}^{+}\Sigma$ is simply given by the metric (1) with the substitution $e^{2\zeta-2\nu}(d\rho^2 + dz^2) \to ds^2/\lambda^2$. If s is the proper radius $\lambda = 1$.

Following the approach for singular hypersurfaces and thin shells initiated by Israel [30,31] (see also Ref. [32] for general charged shells), we define an orthonormal basis tangent to ${}^{+}\Sigma$

$$e^\mu_{(t)} = e^{-\nu}\delta^\mu_t, \qquad e^\mu_{(\phi)} = \frac{e^\nu}{\rho}(\delta^\mu_\phi - A\delta^\mu_t), \qquad (6)$$

$$e^\mu_{(\rho)} = \lambda(s)\left(\rho'(s)\delta^\mu_\rho + z'(s)\delta^\mu_z\right), \qquad (7)$$

where $e^\mu_{(a)} n_\mu = 0$, so that n_μ can used as the tetrad vector $e^\mu_{(z)}$ associated with the z coordinate. The tetrad components of the induced metric are simply

$$\gamma_{(a)(b)} = g_{\mu\nu} e^\mu_{(a)} e^\nu_{(b)} = \text{diag}(-1, 1, 1) \qquad (8)$$

($a, b = \{t, \rho, \phi\}$). The extrinsic curvature is given by the derivative of the normal field along $\Sigma = {}^{+}\Sigma \equiv {}^{-}\Sigma$:

$$K_{(a)(b)} = e^\mu_{(a)} e^\nu_{(b)} \nabla_\mu n_\nu = -n_\nu e^\mu_{(a)} \nabla_\mu e^\nu_{(b)}. \qquad (9)$$

The metric (8) is used to lower/raise indices for 3-tensor quantities, e.g., $K^{(c)}_{(c)} = K_{(a)(b)}\gamma^{(a)(b)}$.

The surface stress-energy tensor which arises due to the identification along the hypersurfaces ${}^{\pm}\Sigma$ with identical induced metrics ${}^{+}g_{(a)(b)} = {}^{-}g_{(a)(b)}$ is given by the difference of the extrinsic curvatures of the hypersurfaces $[K_{(a)(b)}] = {}^{-}K_{(a)(b)} - {}^{+}K_{(a)(b)}$ by the relation [30–32]

$$S_{(a)(b)} = (8\pi)^{-1}\left([K_{(a)(b)}] - \gamma_{(a)(b)}[K^{(c)}_{(c)}]\right). \quad (10)$$

Performing the identification (3), the opposite normals have opposite signs and we get $[K_{(a)(b)}] = -2^{+}K_{(a)(b)}$.

Even though the static tetrad (7) does not exist inside the ergoregions it yields the clearest formulas for the surface stress-energy tensor which arises after the identification (3):

$$4\pi S_{(t)(t)} = 2\nu_{,n} - \zeta_{,n} + (\kappa_1 + \kappa_2)e^{\nu-\zeta}, \quad (11)$$

$$4\pi S_{(\phi)(\phi)} = \zeta_{,n} - \kappa_2 e^{\nu-\zeta}, \quad (12)$$

$$8\pi S_{(t)(\phi)} = \rho^{-1}e^{2\nu}A_{,n}, \quad (13)$$

$$4\pi S_{(\rho)(\rho)} = -\kappa_1 e^{\nu-\zeta}, \quad (14)$$

where $f_{,n} = n^\mu \partial_\mu f = \lambda(\rho' f_{,z} - z' f_{,\rho})$ denotes the normal derivative on Σ^+ and

$$\kappa_1 = \frac{1}{\rho}\frac{z'}{\sqrt{\rho'^2 + z'^2}}, \qquad \kappa_2 = \frac{\rho' z'' - z'\rho''}{(\rho'^2 + z'^2)^{\frac{3}{2}}} \quad (15)$$

are the principal curvatures of the surface given by $t =$ const on the hypersurface ${}^{+}\Sigma$ when considered in flat Euclidean space. Thus, the surface stress-energy tensor is given by a combination of the discontinuities in gravitational potentials and the geometric properties of Σ. An important exception is the radial stress $S_{(\rho)(\rho)}$ which is up to a factor $e^{\nu-\zeta}$ equal to the value of $S^{\text{flat}}_{(\rho)(\rho)}$ in the flat spacetime with $\nu = \zeta = A = 0$. In this sense radial stresses here reflect the external curvature of Σ in flat space rather than the gravitation of sources inside the cutoff region between ${}^{+}\Sigma$. [Notice that the formulas equivalent to Eqs. (11)–(14) but given in a coordinate basis, as in Ref. [10], do not reflect so clearly the respective influences of the gravitational field and of the identification surface.]

In the following we wish to study in detail the properties of the disks without radial pressure. These enable the clearest interpretation of the surface stress-energy tensor. Due to the properties of the WP coordinates which imply Eq. (14) such disks correspond to the hypersurfaces given by $z(s) = b =$ const. Then the surface stress-energy tensor S_{ab}, given in the coordinate rather than tetrad components, simplifies to

$$S_{\alpha\beta} = -\frac{\sqrt{g_{\rho\rho}}}{8\pi}\left(\frac{g_{\alpha\beta}}{g_{\rho\rho}}\right)_{,z}. \quad (16)$$

This form holds only in WP coordinates, and unifies Eqs. (11)–(14). Since in WP coordinates $g_{\rho\rho} = g_{zz}$, the indices $\alpha, \beta = t, \rho, \phi$ can be replaced with $\mu, \nu = t, \rho, z, \phi$ and we get a tensor tangential to the disk hypersurface. Once $S_{\mu\nu}$ is computed in the WP coordinates, we can simply obtain its components in other coordinates or an arbitrary tetrad by appropriate transformations or projections. However, inside the ergoregions we have to either work with coordinate components (16), or use the well-known "zero-angular-momentum" (ZAMO) tetrad (see, e.g., Ref. [33]) rather than Eq. (7) which becomes unphysical there:

$$\tilde{e}^\mu_{(t)} = \frac{g^{1/2}_{\phi\phi}}{\rho}\delta^\mu_t - \frac{g_{t\phi}}{\rho g^{1/2}_{\phi\phi}}\delta^\mu_\phi,$$

$$\tilde{e}^\mu_{(\phi)} = \frac{1}{g^{1/2}_{\phi\phi}}\delta^\mu_\phi, \qquad \tilde{e}^\mu_{(\rho)} = \frac{1}{g^{1/2}_{\rho\rho}}\delta^\mu_\rho, \qquad \tilde{e}^\mu_{(z)} = n^\mu. \quad (17)$$

The method used for the construction of our disk sources guarantees that the values of the total mass M_D and angular momentum J_D of the disks (given by the asymptotic behavior of the metric) are equal to those of the original spacetimes, M and J, provided that the metric satisfies the vacuum Einstein equations outside the disk. Using Komar integrals [33] in stationary axisymmetric spacetimes we can write these quantities as integrals over certain surface densities over the disks (see also Appendix B):

$$M_D = \frac{1}{4\pi}\int_D (2\nu_{,n} + \rho^{-2}e^{4\nu}AA_{,n})\rho\lambda^{-1}(s)dsd\phi, \quad (18)$$

$$J_D = -\frac{1}{8\pi}\int_D \Big[4A\nu_{,n} + A_{,n}(1 + \rho^{-2}A^2e^{4\nu}) + 2A\kappa_1 e^{\nu-\zeta}\Big]\rho\lambda^{-1}(s)dsd\phi. \quad (19)$$

For all spacetimes considered we found that both integrands are also regular inside the ergoregions where $e^{2\nu} < 0$ and individual terms, such as $\nu_{,n} = (e^{2\nu})_{,n}/(2e^{2\nu})$, diverge at circles where the disk source enters the ergoregion.

III. ENERGY CONDITIONS AND THE INTERPRETATION OF THE SURFACE STRESS-ENERGY TENSOR OF THE DISK

For a given solution of the Einstein equations the method we use always provides *some* source. In many cases, however, its properties will be unphysical; for example, it may have a negative energy density or move with superluminal speeds. One way to guarantee physically acceptable sources is to demand that they satisfy some type of suitable energy conditions introduced originally in the studies of the global properties of spacetimes (see, e.g., Ref. [33]). They can be employed without further assumptions about the "material" creating the surface stress-energy tensor $S_{\mu\nu}$. The weak energy condition (WEC) requires, that any observer with velocity W^μ must observe a non-negative energy density $S_{\mu\nu}W^\mu W^\nu$. The dominant energy condition (DEC) is based on the properties of the energy-momentum current $-S_{\mu\nu}W^\mu$, which should be a future-directed timelike vector for classical matter; in fact, DEC $\Rightarrow$ WEC.

It is much easier to decide whether a certain energy condition holds if the stress-energy tensor is in a diagonal form. The diagonalization may be achieved either by finding an observer who measures a diagonal surface stress-energy tensor, or by solving the following eigenvalue problem:

$$(S_{(a)(b)} - \lambda \eta_{(a)(b)})X^{(b)} = 0. \tag{20}$$

Here we assume an arbitrary orthonormal 3-basis satisfying $e^{\mu}_{(a)} e_{\mu(b)} = \eta_{(a)(b)}$ and that the stress-energy tensor has only one off-diagonal component, $S_{(t)(\phi)}$. Then the characteristic equation has real solutions if $(A, B = t, \phi)$

$$\sigma = (S_{(t)(t)} - S_{(\phi)(\phi)})^2 + 4 \det S_{(A)(B)} \geq 0. \tag{21}$$

This inequality is also the necessary condition for the stress-energy tensor to satisfy the weak energy condition, because WEC $\Rightarrow \sigma \geq 0$. [Since $\sigma = (S_{(t)(t)} - 2S_{(t)(\phi)} + S_{(\phi)(\phi)})(S_{(t)(t)} + 2S_{(t)(\phi)} + S_{(\phi)(\phi)}) = (S_{\mu\nu}\xi^{\mu}_1\xi^{\nu}_1)(S_{\rho\sigma}\xi^{\rho}_2\xi^{\sigma}_2)$ for two null vectors $\xi^{\mu}_{1,2} = e^{\mu}_{(t)} \pm e^{\mu}_{(\phi)}$, then, if $\sigma < 0$, one of the two projections of $S_{\mu\nu}$ is negative and, from continuity, there will be observers with velocity near either ξ^{μ}_1 or ξ^{μ}_2 seeing a negative energy density.] From Eq. (20) we obtain three real eigenvalues $-\mu$, $p_{\phi'}$ and p_r where

$$\mu = \frac{1}{2}(S_{(t)(t)} - S_{(\phi)(\phi)} + \sqrt{\sigma}), \tag{22}$$

$$p_{\phi'} = \frac{1}{2}(S_{(\phi)(\phi)} - S_{(t)(t)} + \sqrt{\sigma}), \qquad p_r = S_{(\rho)(\rho)}. \tag{23}$$

The diagonalization yields the tetrad (frame) vectors of the observer with respect to whom the stress-energy tensor is in the diagonal form,

$$\begin{aligned} e^{\mu}_{(t')} &= (e^{\mu}_{(t)} + v e^{\mu}_{(\phi)})/\sqrt{1 - v^2}, \qquad e^{\mu}_{(\rho')} = e^{\mu}_{(\rho)}, \\ e^{\mu}_{(\phi')} &= (v e^{\mu}_{(t)} + e^{\mu}_{(\phi)})/\sqrt{1 - v^2}, \qquad e^{\mu}_{(z')} = e^{\mu}_{(z)}, \end{aligned} \tag{24}$$

where $v = -2S_{(t)(\phi)}/(S_{(t)(t)} + S_{(\phi)(\phi)} + \sqrt{\sigma})$, normalized so that $e^{\mu}_{(\alpha')} e_{\mu(\beta')} = \eta_{(\alpha')(\beta')}$. Then

$$S^{\mu\nu} = \mu e^{\mu}_{(t')} e^{\nu}_{(t')} + p_{\phi'} e^{\mu}_{(\phi')} e^{\nu}_{(\phi')} + p_r e^{\mu}_{(\rho)} e^{\nu}_{(\rho)}. \tag{25}$$

If the decomposition (25) of $S_{\mu\nu}$ is achievable, we can examine $\mu, p_r, p_{\phi'}$ and decide whether the energy conditions are satisfied. The weak energy condition reads

$$\mu \geq 0 \wedge p_r \geq -\mu \wedge p_{\phi'} \geq -\mu, \tag{26}$$

and the dominant energy condition is equivalent to

$$\mu \geq 0 \wedge p_r^2 + p_{\phi'}^2 \leq \mu^2. \tag{27}$$

As we also have the relations

$$\text{WEC} \Rightarrow S_{(t)(t)} + S_{(\phi)(\phi)} \geq 0 \wedge \sigma \geq 0 \Rightarrow |v| < 1, \tag{28}$$

we see that if $\sigma < 0$ or $|v| > 1$ neither energy condition is satisfied.

Instead of the velocity v with respect to an observer equipped with some tetrad frame, we can, as we did in Ref. [9], consider the angular velocity $\Omega = e^{\phi}_{(t')}/e^{t}_{(t')}$ with respect to a static observer at infinity. Regarding the properties of the tetrad basis from which one gets $\sigma = (S_A{}^A)^2 - 4 \det S_A{}^B$, we obtain

$$\Omega = -\frac{2S^{\phi}_{t}}{S^{\phi}_{\phi} - S^{t}_{t} + \sqrt{\sigma}}. \tag{29}$$

In weak gravitational fields this angular velocity gives eigenvector $e^{\mu}_{(t')}$ of (20) and the one with opposite sign in front of $\sqrt{\sigma}$ provides a ratio of ϕ and t components of $e^{\mu}_{(\phi')}$. This may change in the central regions of strong-field disks where one has to check which of the eigenvectors is timelike.

For vanishing radial stresses, $p_r = 0$, the diagonalization described above also yields a possible model of the surface stress-energy tensor of the disks. The equatorial plane can be regarded as being divided into massive circular rings, each with the four-velocity $e^{\mu}_{(t')}$ and the surface energy density μ. These rotating rings (RRs) are supported against the collapse or expansion by their internal azimuthal surface stress $p_{\phi'}$. Although usual materials do not provide $|p|/\mu \lesssim 1$, such high stresses are consistent with energy conditions. In addition, a model more general than RR is not needed—when its diagonalisation is not possible and the surface stress-energy tensor cannot be made of RR, since, due to (28), neither DEC nor WEC holds.

IV. DISKS FROM COUNTER-ROTATING SURFACE STREAMS OF GEODESIC PARTICLES

One of the simplest matter models in general relativity is incoherent dust. To interpret disk sources of *static* spacetimes, Morgan and Morgan [8] introduced the simple model of two counter-rotating geodesic streams (CRGSs) of dust in stationary circular motion. In these static spacetimes no dragging is present and the surface stress-energy tensor is diagonal with two nonzero components, S^{tt} and $S^{\phi\phi}$, with the latter being generated by the velocity of counter-rotating particles. The fact that the velocity which generates the $S^{\phi\phi}$ component matches the Keplerian velocity and the assumed circular motion of counter-rotating particles is consistent with geodesic motion can, as in Ref. [8], be viewed as an implication of the restriction $(S^{t}{}_{t} - S^{\phi}{}_{\phi})\rho\nu_{,\rho} = -S^{\phi}{}_{\phi}$ which Einstein's equations impose on the stress-energy tensor. (The construction of the disk sources of static axisymmetric spacetimes is briefly explained in Appendix A.)

We wish to discuss how the concept of disk surface streams made of counter-rotating particles on circular orbits can be extended to general *stationary* axisymmetric asymptotically flat vacuum spacetimes. Hereafter, we assume that the radial pressure component of the surface stress-energy tensor S_{ab} vanishes (due to the choice $z_\pm = \pm b$). Models of "warm" disks with positive radial pressure were studied in Ref. [10] where material of the disk was described by the distribution function of orbiting particles with various orbital parameters such that their averaged radial motion generates the radial pressure. Clearly, if such a distribution function exists, the energy conditions for the stress-energy tensor [see Eqs. (3.12a)–(3.12d) in Ref. [10]] must hold. However, to get a distribution function describing the population of particles with given orbital parameters requires the solution of complicated integral equations.

As stated above, we assume $p_r = 0$. For positive angular pressure, $p_{\phi'} > 0$, the distribution of orbits is given by a simple model of two streams of counter-rotating circular geodesic dust particles. The nondiagonal metric implies that the surface stress-energy tensor is nondiagonal too and the counter-rotating streams can no longer have identical surface densities and equal and opposite angular velocities. We assume that the disk is composed of two streams of dust particles moving in the plane of identification Σ with velocities $U^\mu_\pm = N_\pm[1, \Omega_\pm, 0, 0]$ and densities $\mu_\pm$, i.e., our stress-energy tensor has the form

$$S^{\mu\nu} = \mu_+ U^\mu_+ U^\nu_+ + \mu_- U^\mu_- U^\nu_-. \tag{30}$$

Here $N^2_\pm = -1/(g_{\phi\phi}\Omega^2_\pm + 2g_{t\phi}\Omega_\pm + g_{tt})$. Both streams are made of particles satisfying geodesic equations which due to symmetries simplify to

$$U^\mu_\pm U^\nu_\pm g_{\mu\nu,\rho} = 0. \tag{31}$$

Equations (30) and (31) represent five equations for four unknown quantities $\mu_\pm$ and $\Omega_\pm$. In an analogy with the static case, the stress-energy tensor is restricted by the Einstein equations (Bianchi identities) so that $S^{\mu\nu}{}_{;\nu} = 0$ (see e.g., Ref. [32]). For a stationary axisymmetric metric this simplifies to $S^{\mu\nu} g_{\mu\nu,\rho} = 0$ and the fact that this linear combination of stress-energy tensor components vanishes means that among the three equations (30) only two are independent.

We thus first solve the radial component of the geodesic equation for the circular geodesic,

$$g_{\phi\phi,\rho}\Omega^2_\pm + 2g_{t\phi,\rho}\Omega_\pm + g_{tt,\rho} = 0, \tag{32}$$

to determine the stream velocities. We must check whether both corotating and counter-rotating angular velocities $\Omega_\pm$ imply timelike vectors. If two subluminal circular geodesics exist, their orbital frequencies $\Omega_\pm$ can be substituted into Eq. (30) from which we find

$$\mu_\pm = \pm(g_{\phi\phi}\Omega^2_\pm + 2g_{t\phi}\Omega_\pm + g_{tt})\frac{\Omega_\mp S^{tt} - S^{\phi t}}{\Omega_+ - \Omega_-}. \tag{33}$$

In the CRGS model, only positive stream densities $\mu_\pm$ are acceptable. The positivity of the stream densities $\mu_\pm$ is related to the sign of the determinant of the 2×2 matrix S^{AB} $(A, B = t, \phi)$, because

$$\begin{aligned}\det S^{AB} &= \rho^{-4} \det S_{AB} = N^2_+ N^2_- \mu_+ \mu_- (\Omega_+ - \Omega_-)^2 \\ &= \mu p_{\phi'} (U^t V^\phi - U^\phi V^t)^2,\end{aligned} \tag{34}$$

with $U^\mu = e^\mu_{(t')}$, $V^\mu = e^\mu_{(\phi')}$. Using the standard criteria for the positivity of the quadratic form S^{AB} we can state that both stream densities $\mu_\pm$ are positive, if $S^{AB}X_A X_B > 0$ for at least one two-component vector X_A, $\det S^{AB} > 0$ and two subluminal solutions $\Omega_\pm$ of (32) exist. Namely, if the RR model yields a disk with positive μ but negative pressure $p_{\phi'}$ somewhere, even if both circular geodesics exist at these radii, one of the counter-rotating streams must have a negative density.

In Ref. [9] we introduced another model of counter-rotating streams; working in the diagonal frame (24), we divided the ring density into two equal-density streams with opposite velocities providing the right value of the pressure $p_{\phi'}$. We did not assume that the particles creating these two streams are in geodesic motion so the necessary condition for this interpretation was $\mu > p_{\phi'} > 0$. As this model assumes some exchange of radial momentum between streams to keep them in circular orbits, in the present work we will prefer the CRGS model of geodesic streams of unequal densities.

The z component of the geodesic equation determines whether a particle located slightly off the disk returns back to the plane of the disk and is thus relevant for the stability of an individual circular orbit. However, we do not address the problem of stability here.

V. TOMIMATSU-SATO SPACETIMES

TS solutions of the Einstein equations were constructed as the generalization of the Kerr solution. Soon after Kerr's discovery, Ernst showed that the Einstein equations for a stationary axisymmetric field are equivalent to a single nonlinear elliptic equation for a complex potential ξ which for the Kerr black-hole solution takes the extraordinarily simple form $\xi = 1/(px + iqy)$ in spheroidal coordinates x, y. [These are simply related to Boyer-Lindquist coordinates, where the parameter q is related to black hole rotation and $p = (1 - q^2)^{1/2}$. A more detailed explanation follows.] Tomimatsu and Sato then showed that there are other solutions of the Ernst equation in the form of complex rational function of x, y representing the field of a localized source [20]. They are labeled by the integer parameter $\delta = 1,2,3,\ldots$ ($\delta = 1$ is Kerr) and the Ernst potential is the quotient of polynomials of degree $\delta^2 - 1$ and δ^2. This yields

asymptotically flat spacetimes with mass M, angular momentum J and quadrupole mass moment Q [20] given by

$$J = M^2 q, \qquad Q = M^3\left(q^2 + \frac{\delta^2 - 1}{3\delta^2}(1 - q^2)\right). \quad (35)$$

The metric potentials appearing in Eq. (1) are then determined by rational functions

$$e^{2\nu} = \frac{L}{E}, \qquad e^{2\zeta} = \frac{L}{F}, \quad \text{and} \quad A = \frac{B}{L}, \quad (36)$$

where L, E, F and B are real-valued polynomials in x, y.

To express $e^{2\nu}, e^{2\zeta}$ and A in the form of rational functions, spheroidal coordinates x, y are needed. They are related to Weyl coordinates ρ, z by the transformation

$$z = \frac{Mp}{\delta}xy, \qquad \rho = \frac{Mp}{\delta}\sqrt{1 - y^2}\sqrt{x^2 - \kappa}. \quad (37)$$

This prescription unifies prolate ($\kappa = +1, |q| < 1$), oblate ($\kappa = -1, |q| > 1$) spheroidal coordinates and spherical coordinates ($\kappa = 0, |q| = 1$). The transformation introduces a scale proportional to the mass M, leaving the coordinates x, y dimensionless. For a given rotation parameter q, the value of the associated parameter p is a positive solution of the equation $\kappa p^2 + q^2 = 1$ (where we choose $p = 1$ for $q = \pm 1$). The introduction of the parameter κ also unifies the expressions for the metric potentials in a way that is equivalent to the complex transformation $p \to -ip$ used in Ref. [20]. For $\delta = 1$ there is a simple relation between the spheroidal coordinates x, y and the Boyer-Lindquist coordinates r, ϑ [34]

$$r = M(px + 1), \qquad \cos\vartheta = y. \quad (38)$$

The WP line element in these unified coordinates (37) reads

$$ds^2 = -e^{2\nu}(dt + Ad\phi)^2 + e^{-2\nu}\rho^2 d\phi^2 + \frac{M^2 p^2}{\delta^2}\frac{x^2 - y^2\kappa}{e^{2\nu - 2\zeta}}\left(\frac{dx^2}{x^2 - \kappa} + \frac{dy^2}{1 - y^2}\right). \quad (39)$$

The key properties of the TS metrics and the coordinates (37) are schematically shown in Fig. 2.

In the stationary WP coordinates (1) the Tomimatsu-Sato spacetimes satisfy the vacuum Einstein equations everywhere apart from singular regions of the coordinates (37) and certain singular rings. These ring singularities (RSs), must be located at roots of the polynomial E (see, e.g., the discussion based on the structure of the curvature invariants in Ref. [23]). As a consequence of the construction from a complex Ernst potential, the polynomial E has the form of a sum of squares of two polynomials, $E = E_1^2 + E_2^2$, so the singularity $E = 0$ occurs at the intersection of the curves $E_1 = 0$ and $E_2 = 0$. Thus, in the x-y or ρ-z plane these singularities are points rather than lines. Then, by also considering the angular coordinate ϕ we get the ring singularities.

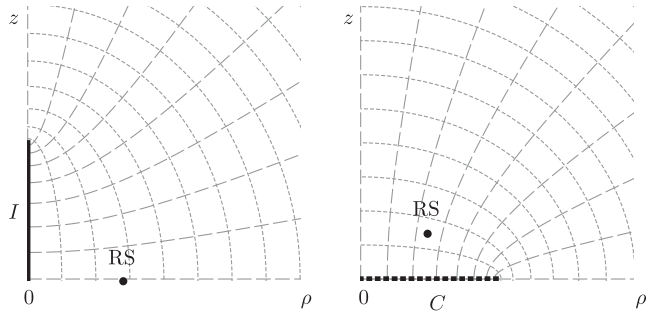

FIG. 2. The prolate (left) and oblate (right) spheroidal coordinates in the ρ-z plane of Weyl-Papapetrou coordinates. Together with lines of constant coordinates x (dashed lines) and y (long-dashed line), the coordinate singularities I and C are plotted. Depending on the value of the TS family parameter δ the line I represents a horizon or a rotating conical singularity with horizons on each end. The cut C can be opened into the coordinate patch $x < 0$. The generic positions of ring singularities for $\delta = 2$ are shown. See text for more details.

For a small rotation parameter $|q| < 1$ the TS metrics require *prolate* spheroidal coordinates. These become singular at $x = 1$. The surfaces of constant x are confocal ellipses in the ρ-z plane which for $x = 1$ reduce to a segment I of the z axis, $z \in [-Mp/\delta, Mp/\delta]$, and the spacetime character of both Killing vectors at the limiting hypersurface I changes with δ. For the Kerr black hole ($\delta = 1, |q| < 1$) the segment I is the event horizon $r = r_+ = (1 + p)M$ and the prolate spheroidal coordinates cover the Kerr spacetime "above" the outer horizon. Similarly, for $\delta = 3$ the segment I is a rotating horizon with regular values for the Weyl invariants [35]. The Killing vector $\partial/\partial\phi$ is timelike on I for even δ. Various analyses of the structure of I for $\delta = 2, |q| < 1$ took many years [22,36], until Ref. [23] showed that the interior of I behaves as a "rotating" conical singularity (known from Newman-Unti-Tamburino spacetime) and the end points of I turn out to be shrunken horizons of spherical shape.

Apart from I, for $\delta = 2$, 3 there is a ring singularity located at the equatorial plane of WP coordinates. Other ring singularities are present in a detached $x < -1$ patch of prolate spheroidal coordinates which we do not consider here (in the Kerr black hole spacetime, this is the well-known RS in the region $r < r_-$).

Another feature appearing in stationary axisymmetric spacetimes are regions of CTCs at places where the Killing vector of the axial symmetry becomes timelike, $g_{\phi\phi} < 0$. In the TS class, only Kerr black hole spacetimes are free of CTCs in the domain of outer communication. Even with $|q| < 1$ for $\delta > 1$ there are toroidal CTC regions (see Fig. 17).

For $|q| = 1$ any $p > 0$ can be chosen and all TS metrics coincide with the extreme Kerr metric. For a large rotation

parameter $|q| > 1$, $\kappa = -1$, *oblate* spheroidal coordinates are required, for which the transformation (37) of the domain $x \in \mathbb{R}, -1 \leq y \leq 1$ covers twice the ρ-z half-plane, where the sheet $x < 0$ has an asymptotically flat infinity with negative mass. For the Kerr spacetime the only RS is located in the equatorial plane $y = 0$ of the $x < 0$ sheet. For TS solutions with a larger δ there are also symmetrically placed off-equatorial pairs of ring singularities. With $|q| > 1$ there are two RSs with $y = 0$, $x < 0$ and one pair of RSs with $x > 0$ for $\delta = 2$, and three RSs with $y = 0$, $x < 0$, one pair of RSs with $x < 0$ and two pairs of RSs with $x > 0$ for $\delta = 3$. The locations of these RSs have not been studied in the literature, because only $|q| < 1$ sources have been discussed in detail, even though, unlike in the Kerr case $\delta = 1$, no cosmic censorship argument favors the $|q| < 1$ case for $\delta > 1$.

While in the construction of disks without the radial pressure we stay in the $x > 0$ region of coordinates, one can in principle enter the $x < 0$ region if disks with nonzero radial pressure are admitted. Unlike in the $|q| < 1$ case where regions of positive and negative x are disjoint in WP coordinates, for $|q| > 1$ the WP metric is regular on the cut $x = 0$. This has the form of a disk $C \coloneqq \{[\rho, \phi, z]; 0 \leq \rho < Mp/\delta, \phi \in [0, 2\pi), z = 0\}$ in WP coordinates. This cut can be understood either as a finite-radius disk source of the given TS spacetime (however, in Sec. VI we show that it would then be made of unphysical matter), or as an entrance into the region of negative x. Some features appearing in the $x > 0$ region as an ergosphere (which can be produced by physical disks) appear to originate at singularities present in the negative x sheet. We illustrate this for the TS solutions with $\delta = 1, 2$ in Fig. 4 where a transformation smoothly covering C is used. Among others, the locations of regions of CTCs in the $x < 0$ sheet of Kerr spacetime are shown. In this figure as well as in Figs. 5, 16, 17 and 18 we use Weyl-Papapetrou coordinates ρ and z scaled in units of M.

VI. PROPERTIES OF DISK SOURCES

In the following we study the disks (without radial pressure so Σ^+ is the hypersurface $z = b$) as sources of the Tomimatsu-Sato spacetimes with mass M, rotation parameter q and an integer distortion parameter $\delta = 1, 2, 3$; the parameter space is illustrated in Fig. 3.

Within this parameter space we explore whether:

(i) the horizon, singularities or CTCs are contained inside the removed region;
(ii) the energy conditions (26) or (27) hold;
(iii) the pressure $p_{\phi'} > 0$ for the RR model;
(iv) real solutions for the circular geodesics of Eq. (32) exist; and
(v) the velocities given by Eq. (32) are subluminal.

First, we note the following useful implications: (iii) $\Rightarrow$ (ii) and (v) $\Rightarrow$ (iv). From Eq. (28) we can also deduce that

(vi) in the RR model, (ii) $\Rightarrow \mu > 0$; and
(vii) in the CRGS model, (ii) $\wedge$ (iii) $\wedge$ (v) $\Rightarrow \mu_\pm > 0$.

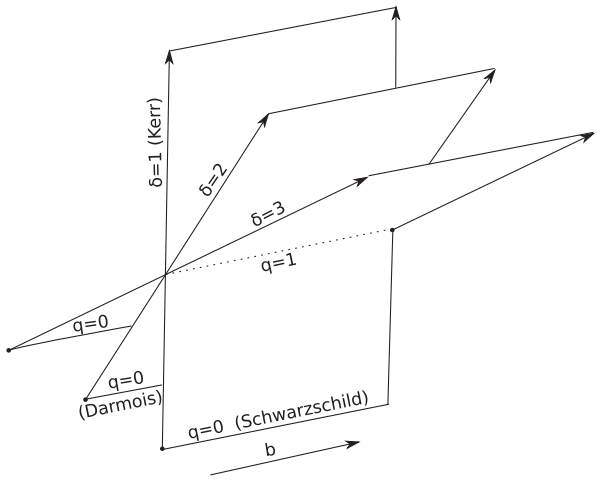

FIG. 3. The schematic picture of the parameter space of disk spacetimes considered. Each disk is characterized by an integer $\delta = 1, 2, 3$ and by its relative angular momentum $q = J/M^2$ (both are the parameters of the original spacetime), and by the size b of the cutoff region. The parameter b determines the compactness of the disk. The mass parameter $M > 0$ is a simple parameter of scale, and one can put $M = 1$. The extreme limit $q = 1$ is the same for any δ.

We also display the properties of the disks described by specific parameters by constructing the plots of the radial dependence of various physical quantities. As a radial coordinate in such plots we use the circumferential radius $R = g_{\phi\phi}^{1/2}$.

To illustrate various densities in the situation when disks and spacetime geometries are very different from a flat geometry, we adopt two approaches. First, we plot cumulative distribution profiles which show what fraction of the Komar mass or of the angular momentum is generated by the central part of the disk below some radius R. Then, we plot the radial profiles of the densities appearing within the Komar integrals. For our disks with $z(s) = b$, we write the integrals (18) and (19) over the surface densities μ_D, j_D defined with respect to the circumferential radius R as

$$M_D = \int_0^\infty \mu_D 2\pi R dR, \qquad \mu_D = \frac{2\rho g_{\rho\rho}^{1/2}}{g_{\phi\phi,\rho}}(S_\phi^\phi - S_t^t), \tag{40}$$

$$J_D = \int_0^\infty j_D 2\pi R dR, \qquad j_D = \frac{2\rho g_{\rho\rho}^{1/2}}{g_{\phi\phi,\rho}} S_\phi^t. \tag{41}$$

This approach also enables us to assign the densities $\mu_D^\pm$ to both counter-rotating streams in Eq. (30); their radial integrals then determine how much of the total (Komar) disk mass is generated within each stream.

A. The disk sources of the Tomimatsu-Sato spacetimes

In this section we use the general results given above to construct the disk sources of the Tomimatsu-Sato spacetimes. Let us define the "derivative operation" denoted by "$\prime$" acting on a function $f(x, y)$ as

$$f' = (x^2-\kappa)\frac{\partial f}{\partial x} + (1-y^2)\frac{x}{y}\frac{\partial f}{\partial y}. \tag{42}$$

The ∂_z derivative appearing in the general formula for the surface stress tensor (16) can be expressed as

$$\frac{\partial f}{\partial z} = \frac{\delta}{Mp}\frac{y}{x^2-\kappa y^2} f'. \tag{43}$$

Then, employing this operation, we find that the surface stress-energy tensor components (16) in the TS metrics read

$$S_{tt} = \frac{ZLF}{E^2}\left(\frac{L'}{L}+\frac{F'}{F}-2\frac{E'}{E}\right), \tag{44}$$

$$S_{t\phi} = \frac{ZBF}{E^2}\left(\frac{B'}{B}+\frac{F'}{F}-2\frac{E'}{E}\right), \tag{45}$$

$$S_{\phi\phi} = \frac{ZF}{L}\left[\left(\rho^2-\frac{B^2}{E^2}\right)\left(\frac{L'}{L}-\frac{F'}{F}\right) + 2\frac{B^2}{E^2}\left(\frac{B'}{B}-\frac{E'}{E}\right)\right], \tag{46}$$

where a substitution has to be made for x and y from Eq. (37) so that the expressions become functions of the coordinate ρ in the plane $z = b$ of the disk, and

$$Z = \frac{1}{8\pi}\frac{\delta}{Mp}\sqrt{\frac{E}{F}}\frac{y}{x^2-\kappa y^2}. \tag{47}$$

For vacuum spacetimes the only realistic case in the TS family is the Kerr black hole spacetime with $|q| \leq 1$; otherwise naked singularities occur in the central regions. In our approach the central parts are replaced by a disk and the value of q itself is not directly restricted by the presence of naked singularities in the complete solution. Instead, the size of the region between Σ^- and Σ^+ that must be excluded is determined by the properties of the disk, namely, whether the energy conditions hold or if the cutoff region admits the particular model of the disk matter (such as RR or CRGS).

For the Tomimatsu-Sato spacetimes with small angular momentum J and identifications performed at large b, both the disk sources and the fields will be weak and similar to the Schwarzschild-disk cases [3]. For such disks both the RR and CRGS interpretations are possible.

The CRGS model requires a positive value of the determinant (34) and this condition may be broken even in the weak-field limit $b \gg M$, when pressures are still small, but negative. Using the expansion of the TS metric functions we can find an approximate expression for Eq. (34) and check its sign. It turns out that the spacetime geometry prohibits CRGS disk sources for large enough angular momentum since negative pressures $p_{\phi'}$ appear near the axis. In this approximation both CRGS densities are positive only if $b/M \gtrapprox 2 + 9q^2/4 \gg 1$, or, expressed in terms of the disk mass and angular momentum, [20]

$$b \gtrapprox 2M + \frac{9J^2}{4M^3} \wedge b \gg M. \tag{48}$$

In the higher-order approximation the quadrupole moment (which also depends on δ) enters this formula.

Since the Kerr solution is a member of the TS family we should mention some implications which the last conditions bear on the cosmic censorship conjecture. This admits only the formation of the Kerr black holes which have $|q| \leq 1$. Although the construction of the disk sources does not in principle prevent us from constructing the TS spacetimes with $|q| > 1$, there is a "barrier" which disfavors the construction of even mildly compact CRGS disk sources with large q. If the ratio M/b is taken as a field-strength indicator, in the Kerr case ($\delta = 1$) we have $M/b \lessapprox 4/(9q^2)$. In this sense, a "parametric collapse" of a CRGS disk into a naked Kerr singularity is prohibited already at early stages.

As b becomes smaller, the relativistic effects play more a important role and at some point truly strong-field features may prevent the disk source from having physically plausible properties: one of the circular Keplerian geodesics may become superluminal, or the energy conditions may be violated (either S^{ab} cannot be diagonalized or the energy density of the RR becomes negative at some radii). For the set of spacetimes we consider, it was confirmed that unless the energy conditions are violated, *closed timelike curves do not exist in the spacetime surrounding the disk*. Disks that are compact enough, with parameters close to extreme black holes, exhibit the presence of the ergoregions in the vicinity of the disk but because at least one of $\Omega_\pm$ is tachyonic there, *only disks made of RR can be surrounded by a toroidal ergoregion*.

As shown in Fig. 4 for the Tomimatsu-Sato $q > 1$ spacetime, the identification along the surface $z = \text{const}$ could in principle reveal parts of the spacetime with CTCs extending to a distant observer. The extension into negative values of the coordinate z shown in this figure for $|q| > 1$ were discussed in e.g., Ref. [37], or more recently, in Refs. [38,39]. In the following sections we show that for TS $\delta = 2$, 3 spacetimes the energy conditions are violated already before the CTC domain appears around the disk. This illustrates a certain "parametric form" of the chronology protection conjecture in general relativity.

B. Kerr ($\delta = 1$) disks

The most important solution in the TS family is the Kerr metric with the metric functions

$$e^{2\nu} = \frac{p^2(x^2-\kappa) - q^2(1-y^2)}{(px+1)^2 + q^2y^2}, \tag{49}$$

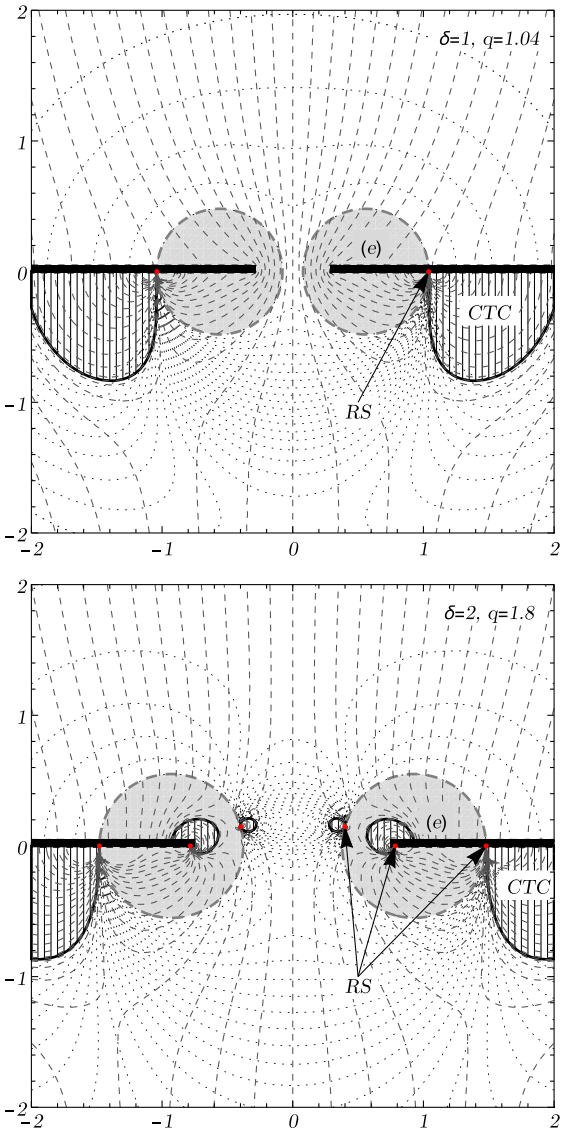

FIG. 4. For $|q| > 1$ the oblate spheroidal coordinates can be simply extended to the patch $x < 0$. When plotted in ρ-z plane in Weyl-Papapetrou coordinates this extension yields a cut in the $z = 0$ plane along $\rho > Mp/\delta$ (thick horizontal line) so that the standard region ($x > 0$) is in the upper part and the extended ($x < 0$) region is in the lower part of the plot. To show rotational symmetry, we extend ρ symmetrically in the left half of the plot. The toroidal ergosphere (e), CTC regions and ring singularities of $|q| > 1$ Kerr (top) and TS $\delta = 2$ (bottom) spacetimes are illustrated in this figure. The identifications along $z = \pm b$ can provide disk sources with ergoregions for the Kerr case, and for $\delta > 1$ disks can also be surrounded by toroidal regions of CTCs. Contours show the norms of Killing vectors, $g_{tt} = -0.1, -0.2, \ldots$ (dotted) and $R = g_{\phi\phi}^{1/2} = 0, 0.25, 0.5, \ldots$ (dashed).

$$e^{2\zeta} = \frac{p^2(x^2-\kappa) - q^2(1-y^2)}{p^2(x^2-\kappa y^2)}, \tag{50}$$

$$A = \frac{2Mq(1-y^2)(1+px)}{p^2(x^2-\kappa) - q^2(1-y^2)}. \tag{51}$$

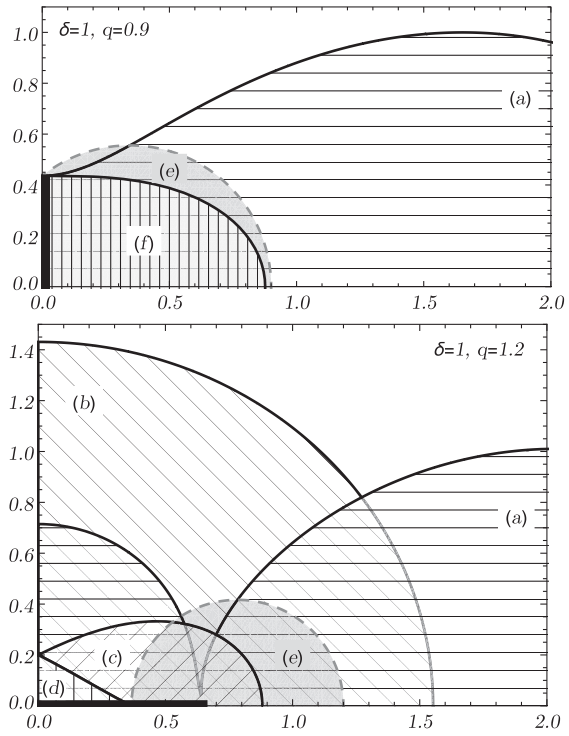

FIG. 5. Properties of the stress-energy tensor of a $p_r = 0$ disk as a source of the Kerr geometry in the ρ-z plane of Weyl-Papapetrou coordinates for a $M = 1$ Kerr black hole (top) and Kerr naked singularity (bottom). To determine these properties one draws a horizontal line $z = b$ (corresponding to the identification surface Σ^+) and along this line reads out the properties of the stress-energy tensor at given radius of the disk: (a) one or both Keplerian velocities are superluminal; (b) a negative value of $\det S_{AB} \sim \mu p_{\phi'} \sim \mu_+\mu_-$; (c) no diagonalization is possible, $\sigma < 0$; (d) the energy density μ of RR is negative; (e) an ergosphere; (f) a pressure exceeding the DEC limit, $p_{\phi'} > \mu$.

When the radial pressure-free disks with $\Sigma^+ = \{x^\mu | z = b\}$ with $|q| \leq 1$ are constructed as sources of the Kerr metric, the excluded ("cutoff") region must satisfy the condition $b > Mp$ so that the horizon is completely removed from the disk spacetime. For $|q| > 1$ the ring singularity lies in the $x < 0$ patch of coordinates so any $b > 0$ is in principle permissible. The singular region of the prolate spheroidal coordinates which coincides with the Kerr black hole horizon, and that of oblate spheroidal coordinates, through which the patch $x < 0$ can be reached, are shown as thick black solid lines in Fig. 5. This is plotted for the "black-hole" and "naked Kerr" rotation parameters $q = 0.9$ and $q = 1.2$, respectively and the properties of the disk stress-energy tensor for various values of the parameter b and radial coordinate ρ are shown.

Kerr black-hole metrics. The properties of disk sources with $|q| < 1$ are illustrated in the top panel of Fig. 5. One can construct RR disks with $|q| < 1$ as long the whole black-hole horizon (thick vertical line in the figure) is contained between Σ^+ and Σ^-, i.e., $b > Mp$ must be

chosen. If the disk were to "cut into" the horizon, the radially "static" matter of RR would need a pressure $p > \mu$ near the horizon.

For $1/\sqrt{2} < q < 1$, spacetimes of compact enough RR disks may contain an ergoregion (light gray regions in the figure). The dashed region (a) shows places where two timelike counter-rotating circular geodesics in the plane $\Sigma^{\pm}$ do not exist and the disks cannot be made of CRGS. For $q < 1$ this effect restricts the disk compactness to $b \gtrsim M$.

Naked Kerr metrics: For $|q| > 1$ more obstacles to construct disk sources arise as can be seen in the bottom panel of Fig. 5. We already mentioned region (a) in which we do not have the counter-rotating circular geodesics needed to construct the CRGS surface stress-energy tensor (30). For $a > M$ this region also spreads along the z axis. Even if both geodesics exist, realistic CRGS models cannot have negative stream densities, which happens in region (b). For $q \gtrsim 1.12$ the positivity of stream densities restricts possible central redshifts more strictly than the existence of timelike CRGS geodesics. Still, the RR disk model is possible until the value of b reaches the region (c). Then we cannot diagonalize the disk stress-energy tensor and both the WEC and DEC are violated.

For disks with even stronger fields (when $b < a - M$), we find that near the disk center a negative energy density arises [region (d)]. At the same threshold, $b < a - M$, a repulsive force starts to act on the particle at the disk center. For a discussion of the repulsive effects of the naked Kerr singularity, see, e.g., Ref. [40].

Disk compactness restrictions: due to the centrifugal effects are shown in the top panel of Fig. 6. There, for $\delta = 1$, 2, 3, and for given q, we plot the minimal values of the parameter b, for which the considered properties of the Kerr disk stress-energy tensor hold for $\rho \in [0, \infty)$. We analyze disks with $|q| < 2$ and $b/M < 2$ by dividing the parameter space into the following regions indicated in Fig. 6.

RR and CRGS: When a large enough central region is removed by the identification, the stress-energy tensor can be interpreted using both the RR and CRGS models. Their properties are discussed in detail in the following text.

RR$^-$: For given disk parameters, the RR model is applicable, but at certain disk radii there is a negative value of $p_{\phi'}$. Then, even if both circular geodesics exist, one of the stream densities would have to be negative as follows from Eq. (34). The upper boundary of the region is approximately described by the relation (48); an exact, but rather lengthy formula is given in Ref. [9].

RR$^+$: The RR model is applicable, as both μ and $p_{\phi'}$ are non-negative everywhere. Disks cannot be made of CRGS because two timelike circular geodesics are not available at some radii.

$\overline{\text{WEC}}$: At some disk radii the surface stress-energy tensor cannot be diagonalized, or the obtained energy

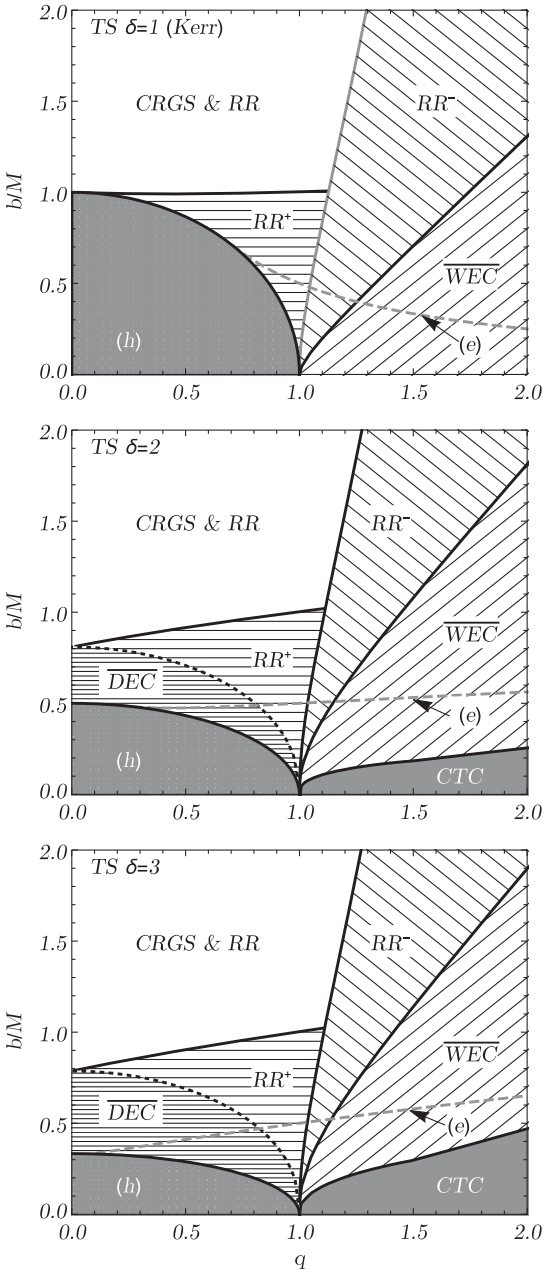

FIG. 6. Properties of disks with given angular momentum parameter q and half-width of the excluded region b generating TS metrics with $\delta = 1$, 2, 3. For large enough b both RR and CRGS models are applicable. For given b when increasing the angular momentum we enter the RR$^-$ region where at some disk radii, negative tangential pressure appears. For smaller b counter-rotating circular timelike geodesics no longer exist and we enter the RR$^+$ region where RR have positive pressure everywhere. In the $\overline{\text{WEC}}$ region of parameters, either the rings have negative mass density or the stress-energy tensor cannot be diagonalized. In the $\overline{\text{DEC}}$ region the pressure exceeds the RR density at some radii. Disks with parameters below region (e) have ergoregions, while those in region (h) or CTC touch the horizon or involve CTCs.

density μ is negative. The weak and dominant energy conditions are violated.

$\overline{\text{DEC}}$: At some radii $p_{\phi'}$ exceeds the energy density μ, and thus the dominant energy condition is violated. For $\delta = 1$ this region is completely covered by (h).

CTC: The region excluded by the identification is not large enough to contain all CTC regions. Ring singularities may appear above the disk for even smaller b. (This can happen only for $\delta \geq 2$.)

(**h**): The region excluded by identification is not large enough to contain the horizon.

(**e**): An ergosphere occurs above the disk; this is possible for the RR disks with $q \approx 1$.

Among the disks considered, only the Kerr $\delta = 1$ disks for $|q| \leq 1$ can have arbitrarily large central redshifts and satisfy the energy conditions; these are the disks with parameters q, b at the boundary of region (h) in Fig. 6. The CRGS model yields arbitrarily large central redshifts only for the Schwarzschild disk with $q = 0, b \searrow M$.

In Fig. 7 we illustrate the mass distribution inside the disks by expressing the relative mass contribution, $M_K(R)/M$, of the central part of the disk up to a given radius R, to the total Komar mass (19). Since the leading term of the asymptotic behavior depends only on the mass parameter, at large radii we get the same profile as for the classical Kuzmin disks with $M_K(R)/M \doteq 1 - b/R$, independently of the parameters δ and q. The distribution changes only slightly with the TS parameter δ as is also illustrated in Fig. 7. The distribution of the angular momentum is shown in Fig. 8.

In order to interpret the nondiagonal stress-energy tensor $S_{(a)(b)}$, we introduced the observers (24) with respect to whom the stress-tensor becomes diagonal [such observers

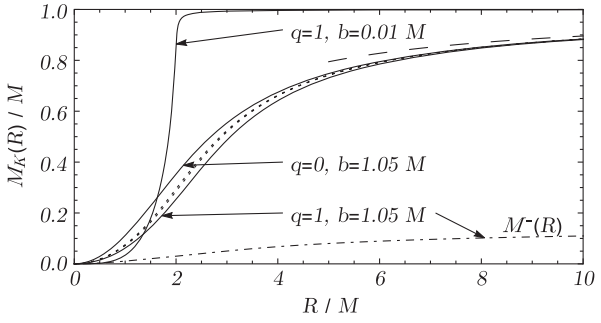

FIG. 7. Cumulative radial distribution of the Komar mass inside the Kerr disks as a function of circumferential radius R. For $q \approx 1$, disks with a compact mass distribution are possible; for the CRGS models we have to choose $b \gtrapprox M$ and the disk matter is more spread out. Mass fractions of the $b = 1.05M$ Newtonian Kuzmin disk models are shown as a long-dashed line. For $q = 1, b = 1.05M$, both CRGS have positive densities but the μ^- component [dash-dotted line $M^-(R)$] is responsible for only about 15% of the total Komar mass of the disk. Dotted lines between the $q = 0$ and $q = 1$ lines show profiles of $q = 0, b = 1.05M$ disks with $\delta = 2$ and $\delta = 3$ (top to bottom).

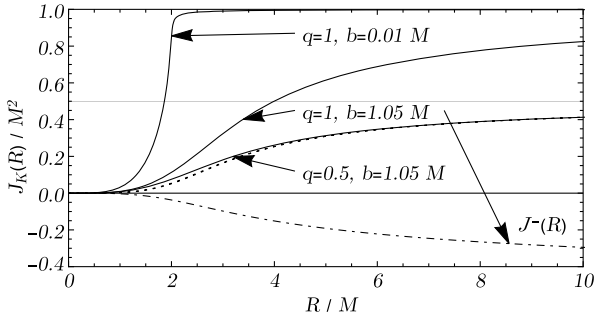

FIG. 8. Cumulative radial distribution of the Komar angular momentum inside the Kerr disks as a function of circumferential radius R. For the parameters $q = 1, b = 1.05M$ a negative angular momentum due to μ_- carrying about -57% of the total angular momentum is also shown (dash-dotted line), while the remaining 157% is deposited in the corotating stream. Dotted lines below the $q = 0.5$ line show profiles of $q = 0.5, b = 1.05M$ disks with $\delta = 2$ and $\delta = 3$ (top to bottom).

were called FIOs ("ϕ-isotropic") in Ref. [9]]. In Fig. 9 we show their angular velocity (29) for several disk parameters. For a compact enough disk with $q > 1$ we find that the angular velocity slightly surpasses that of the horizon of an extreme Kerr black hole. However, if the stress-energy tensor can be diagonalized we do not reach $\Omega \gtrsim 0.69/M$. This angular velocity determines the speed of rotation of the RR disk source the properties of which are shown in Fig. 10. Since the parameters were chosen to describe strong-field disk sources we can see considerable differences between μ and μ_D, and we also find a disk with a large negative pressure $p \approx -\mu$.

The properties of the disks made of CRGS are shown in Fig. 11. For two disk models with quite different parameters q and b we illustrate the effects of the rotational dragging. It may force both geodesic streams' orbits to rotate in the same direction with respect to infinity. Also, the stream densities differ significantly as is shown in Fig. 12. For given mass and angular momentum of the disk, we can obtain disks of various compactness by varying the parameter b. For larger values of b dragging soon disappears, stream velocities become symmetric, $\Omega_- \approx -\Omega_+$,

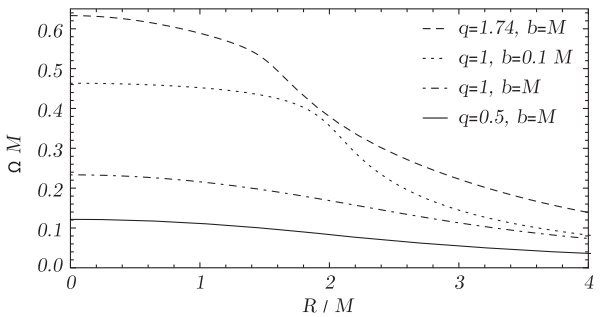

FIG. 9. Angular velocity of frames with the diagonal form of the disk surface stress-energy tensor. The chosen values of the parameters q and b imply disks which in some regions cannot be formed by CRGS.

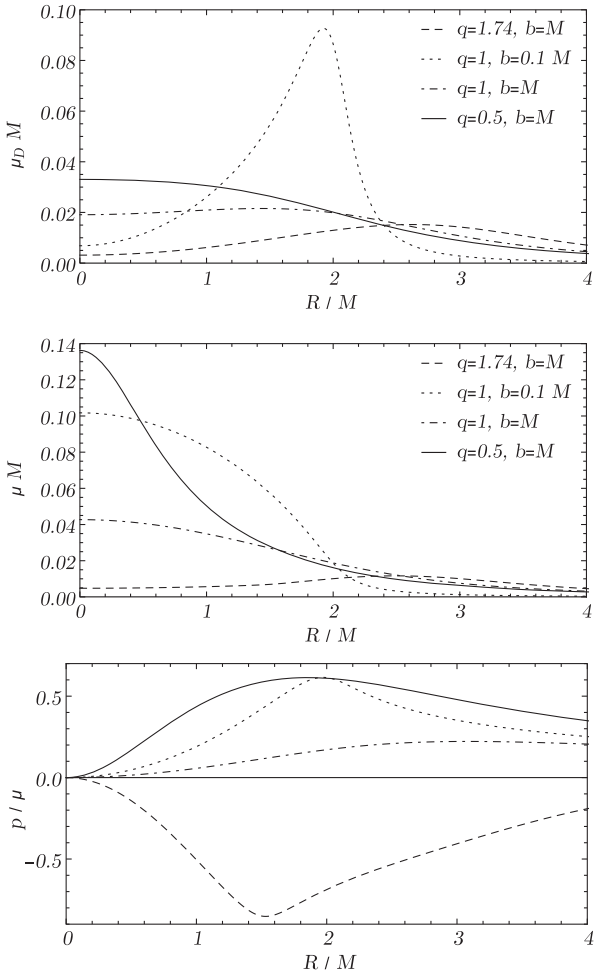

FIG. 10. Komar mass density μ_D (top), stream density μ (middle) and the ratio p/μ (bottom) for several Kerr disks.

and the net angular momenta of disks are due to the difference between μ_+ and μ_-.

C. Extreme Kerr disks

The extreme Kerr black hole spacetime with $q = 1$ is worthy of a separate discussion. Many expressions

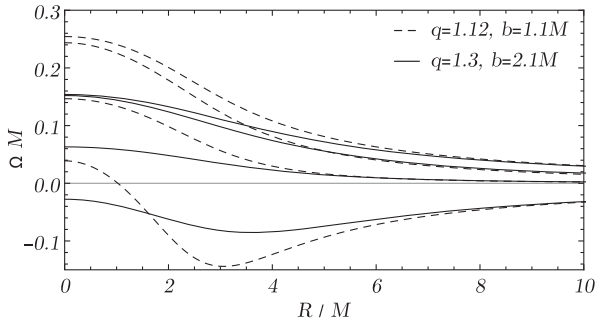

FIG. 11. Angular velocities (from top to bottom) of the corotating geodesic stream Ω_+, isotropic observer Ω, zero angular momentum observer Ω_{ZAMO}, and counter-rotating geodesic stream Ω_- for two CRGS disk models.

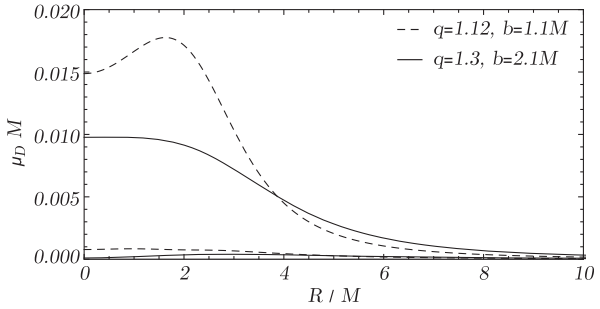

FIG. 12. Komar mass densities of corotating (upper curves) and counter-rotating (lower curves) streams. Both sets of parameters q and b are chosen close to the limit when the counter-rotating stream density becomes negative. For the chosen parameters the Komar mass of the counter-rotating components is only about $M/8$.

simplify, the condition (21) is always satisfied and for the RR model we can write explicitly the energy density, pressure and velocity with respect to the ZAMO (17) as follows:

$$\mu = \frac{y}{4\pi M}\frac{w + x + 2y^2}{[(x+1)^2 + y^2]^{3/2}}, \tag{52}$$

$$p_{\phi'} = \frac{y}{4\pi M}\frac{w - x - 2y^2}{[(x+1)^2 + y^2]^{3/2}}, \tag{53}$$

$$v_{\mathrm{ZAMO}} = \frac{\sqrt{1-y^2}}{w + x + 2}\frac{2 + x(2x + 4 + w)}{2 + x(2x + 4 - w)}, \tag{54}$$

where $w = \sqrt{x(x+4) + y^2 + 3}$.

Also, only in the extreme Kerr case can we remove the arbitrarily "thin" region between the hypersurfaces ${}^-\Sigma$ and ${}^+\Sigma$, i.e., consider the limit $b \to 0$, since for $0 \le q < 1$ we would hit the horizon of the black hole and for $q > 1$ the energy conditions would be violated for small b, and with the parameter $\delta > 1$ singularities would appear outside the disk (see Fig. 6). The RR disks with $q = 1$ properties are illustrated in Fig. 13. There we see that the limiting case is a finite-radius disk (cf. also Fig. 7). Figure 14 shows that such a disk rotates rigidly with angular velocity equal to the horizon angular velocity of an extreme Kerr black hole, $M\Omega_H = 1/2$. Similar behavior was observed in Ref. [41] for disks made of rigidly rotating dust. In Fig. 15 the shape of $z = \mathrm{const}$ surfaces is shown in Boyer-Lindquist coordinates R_{BL}, θ. One can check there that in the limiting case the extreme Kerr black hole is removed by the identification of mirrored points just above the extreme horizon ($R = 2M$ is the circumferential radius of the extreme horizon).

D. Tomimatsu-Sato $\delta = 2$ disks

The TS spacetime with $\delta = 2$ (TS2) is determined by the mass M and angular momentum $M^2 q$ [42]. The parameter p again satisfies the relation $\kappa p^2 + q^2 = 1, \kappa = \pm 1$. Introducing

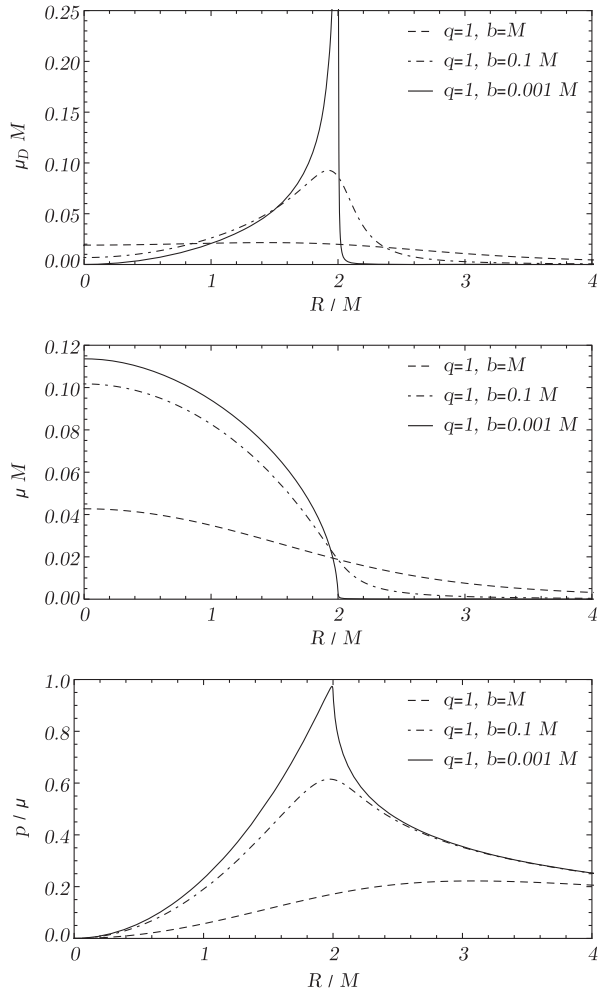

FIG. 13. Komar mass density μ_D (top), RR stream density μ (middle) and the ratio p/μ (bottom) for extreme Kerr disks for $b/M = 1$, 0.1, 0.001.

the abbreviations $a=x^2-\kappa$, $b=1-y^2$, $c=(\kappa p^2(x^4-1)-q^2(1-y^4)+2px\kappa a)$, and $d=p^3xa(2(x^4-1)+(\kappa x^2+3)b)$, the line element is given by Eq. (1), where

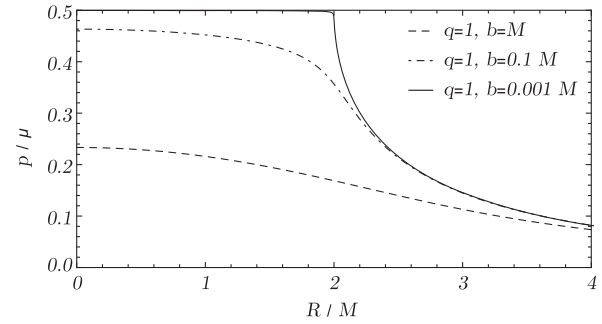

FIG. 14. Angular velocity with respect to infinity of rotating-ring sources of extreme Kerr disks. When $b \to 0$ all of the disks' mass is located below $R = 2M$ and the rings exhibit rigid-body rotation with angular velocity equal to the horizon angular velocity of an extreme Kerr black hole $M\Omega_H = 1/2$.

$$e^{2\nu} = \frac{p^4a^4+q^4b^4-2p^2q^2ab(2a^2+2b^2+3\kappa ab)}{c^2+4q^2y^2(px\kappa a+(px+1)b)^2},$$
$$e^{2\zeta} = \frac{p^4a^4+q^4b^4-2p^2q^2ab(2a^2+2b^2+3\kappa ab)}{p^4(x^2-\kappa y^2)^4}, \quad (55)$$
$$A = 2Mqb\frac{-d-(4ax^2+(3\kappa x^2+1)b)ap^2+q^2(px+1)b^3}{p^4a^4+q^4b^4-2p^2q^2ab(2a^2+2b^2+3\kappa ab)}.$$

These metric potentials are written down in the short form which assumes $\kappa^2 = 1$ and thus they do not include the extreme ($q = 1$) case, which is identical to the extreme Kerr metric. This can be shown by putting $\kappa=1$, $x=\hat{x}\delta/p, q=1$ and then taking the limit $p \to 0$.

The static limit $q = 0$ of the TS2 spacetime is the Darmois solution (the Weyl metric with a metric potential ν proportional, by a factor of 2, to the metric potential of the Schwarzschild solution with mass $M/2$), and the corresponding disk source were thus studied as a special case of Zipoy-Voorhees metrics in Ref. [3].

As mentioned in Sec. V, one of the most important differences between the Kerr and TS2 families is that in the TS2 spacetime for $|q| > 1$ there remain both singular rings and toroidal regions of closed timelike curves outside the equatorial plane. We limit the choice of the identification hypersurface in such a way, that singularities remain in the removed region.

In Fig. 16 we illustrate the properties of the stress-energy tensor of the TS $\delta = 2$ disks for two values of the parameter q, namely $q = 0.8$ and $q = 1.2$. For $|q| < 1$ we observe DEC violation in region (f) as we approach the poles of the horizon. For $|q| > 1$ we see how for smaller values the RR model is not admissible because at some radii we cannot diagonalize the disk stress-energy tensor; this also indicates WEC violation. In both the $|q| < 1$ and $|q| > 1$ cases we also see how for an incomplete set of timelike circular geodesics in the plane of the disk, region (a) disfavors the CRGS model, which is, for $|q| > 1$ even more strictly limited by the region of negative pressure (b), which, due to Eq. (34), implies that one of the counter-rotating geodesic streams has a negative density. These properties are summarized for $0 < q < 2$ in the middle panel of Fig. 6 where the dependence of the disk properties on the rotation parameter is illustrated.

E. Tomimatsu-Sato $\delta = 3$ disks

For $\delta = 3$ the metric potentials are given by rather lengthy expressions [20]; however, even though the central region fields are thus more complicated, the existence of both RR and CRGS disks is restricted already in weaker-field regions where the properties of the disk surface stress-energy tensors for $\delta = 2$ and $\delta = 3$ are analogous. The regions of parameters q and b where RR or CRGS models are applicable (see Fig. 6) are very similar. We compare side by side the disk features for $\delta = 2$, 3 in Figs. 17 and 18. These cover the

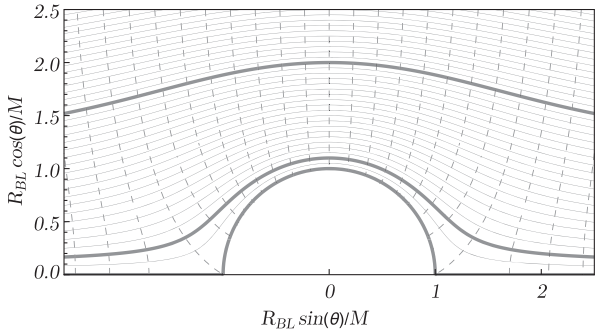

FIG. 15. Shape of the $z = \text{const}$ identification surfaces in Boyer-Lindquist coordinates for an extreme Kerr black hole. The thick lines represent the values $z/M = 1,\ 0.1,\ 0.001$ considered in Fig. 13. Dashed lines are places of constant circumferential radius $R/M = 0, 0.25, 0.5, \ldots$

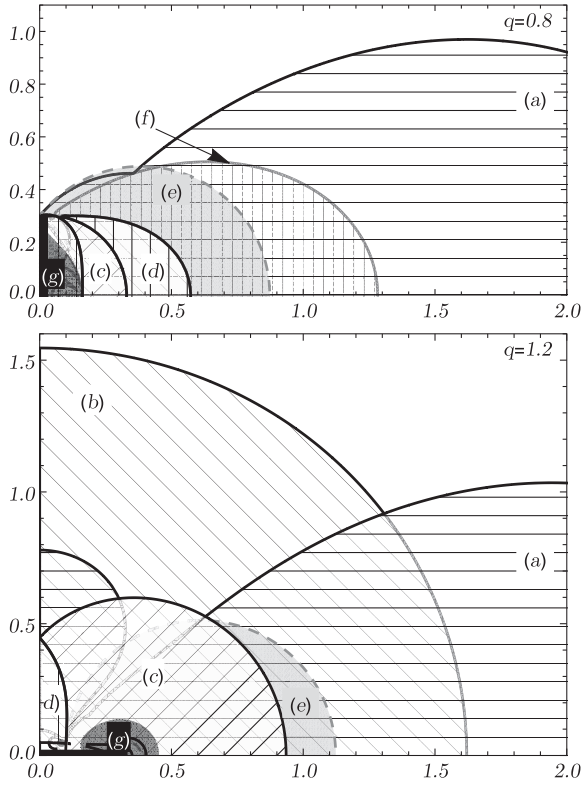

FIG. 16. Properties of the stress-energy tensor of a $p_r = 0$ disk as a source $\delta = 2$, $M = 1$ Tomimatsu-Sato geometry in the ρ-z plane in Weyl-Papapetrou coordinates for $q = 0.8$ (top) and $q = 1.2$ (bottom). When the identification surfaces $\Sigma^{\pm}$ are fixed by the prescription $z = \text{const}$ (which would appear as two horizontal lines in the ρ-z plane) the plots show properties of the stress-energy tensor at a given radius of the disk: (a) one or both Keplerian velocities are superluminal; (b) a negative value of $\det S_{AB} \sim \mu p_{\phi'} \sim \mu_+\mu_-$; (c) no diagonalization is possible, $\sigma < 0$; (d) the energy density μ of RR is negative; (e) an ergosphere; (f) the pressure exceeds the DEC limit, $p/\mu > 1$; and (g) closed timelike curves.

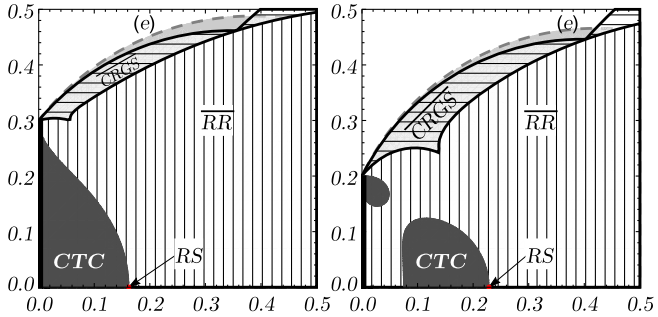

FIG. 17. A detailed view of the properties of disk sources with $\delta = 2$ (left) and $\delta = 3$ (right) for $q = 0.8$. The panels show the central, strong-field region in the ρ-z plane in Weyl-Papapetrou coordinates, $M = 1$. All reasons why the disks cannot be made of RRs and CRGSs are considered and only combined regions where RR or CRGS models are not admissible are shown. From the other features of the spacetime, only the ergosphere (e) and the region of closed timelike curves (dark gray) is shown. Arrows indicate the positions of ring singularities.

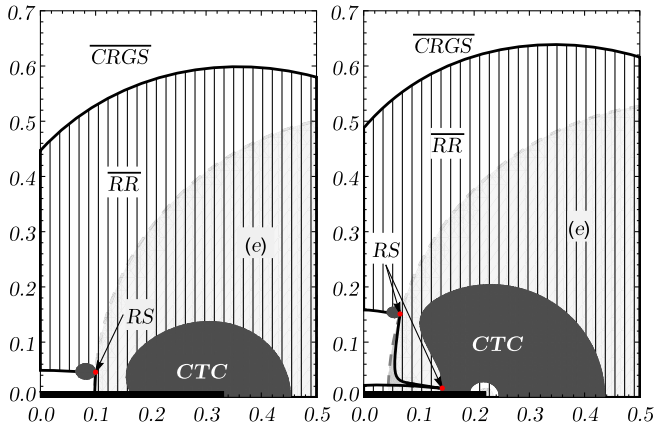

FIG. 18. A detailed view of the properties of disk sources with $\delta = 2$ (left) and $\delta = 3$ (right) for $q = 1.2$. The panels show the central, strong-field region in the ρ-z plane in Weyl-Papapetrou coordinates, $M = 1$. In the displayed range of the coordinate z, the stress-energy tensor cannot be made of CRGS. Otherwise, the caption of Fig 17 applies here too.

central regions of the ρ-z plane in Weyl-Papapetrou coordinates, outside of which the properties of $\delta = 3$ disks are very similar to those of $\delta = 2$ disks shown in Fig 16.

VII. CONCLUSIONS

The properties of the sources of stationary vacuum axisymmetric spacetimes were analyzed by considering material disks which arise from suitable identifications of two hypersurfaces. We showed that at a given point of the disk source the only degrees of freedom are the two principal curvatures of the surface of identification. Choosing these to be zero yields disks without radial

pressure. Since disks have no interiors we obtained a direct relation between the properties of the disk sources and metric potentials and their first derivatives. This enabled us to identify regions where certain features of the disk stress-energy tensor hold for a given spacetime. We chose the first three members of the Tomimatsu-Sato family. Our approach is thus an extension of an analysis of such spacetimes where the metric and its derivatives are used to find the causal structure, to describe the geodesic motion and to identify the presence of singularities.

The method of the construction by suitable identification enabled us to avoid the pathological "central regions" and obtain completely regular spacetimes outside of the disks. The discontinuities in the first derivatives of the metric then represent material sources with plausible physical properties. The resulting disks have infinite radii but most of their mass appears near their center which is similar to the disk models of galaxies. Each disk source is parametrized by the properties of the corresponding spacetime: mass, angular momentum, the TS family index δ and the parameter determining how large of a portion of a spacetime is replaced by the disk source.

The symmetries of spacetimes admit two interpretations of the surface stress-energy tensor of the disk with vanishing radial pressure. When the surface stress-energy tensor satisfies the weak energy condition, we can consider that the model of the rings defies the gravitational forces by their tangential pressure. Each ring rotates with an appropriate angular velocity which is the implication of the frame dragging and is the source of angular momentum. A mechanism which generates this pressure was not considered. When both corotating and counter-rotating circular timelike geodesics exist in the plane of the disk, the stress-energy tensor satisfies the energy conditions and has a positive tangential pressure; rather surprisingly, both circular streams may be endowed with appropriate positive densities and the Einstein equations then guarantee that these two densities can provide all three nonzero components of the disk surface stress-energy tensor. Differences in the stream densities and velocities appear as the source of the net angular momentum.

The results show that for a given Tomimatsu-Sato spacetime we can construct disks using both models if we exclude a large enough region containing pathologies such as horizons, branching surfaces, naked singularities and closed timelike curves. We can see the influence of centrifugal effects for disks with large enough angular momentum which do not allow highly compact disks formed of counter-rotating geodesic streams with angular momentum $J \gg M^2$. Also, we provided another example when the extreme Kerr spacetime is confirmed as a limiting case for very compact extremely rotating disks. Since the spacetimes studied in this work contain regions of closed timelike curves we may consider a parametric collapse of the disk into the state when a region with CTCs would appear above the disk. We then observed that the energy conditions are violated *first*, before CTCs appear.

ACKNOWLEDGMENTS

T. L. and J. B. acknowledge partial support from the Grant GAČR No. 17-13525S of the Czech Republic. During the final preparation of the paper, J. B. was a visiting fellow at the Institute of Astronomy in Cambridge and at the Albert-Einstein Institute, Golm. We are thankful for the kind hospitality of R. G. McMahon and L. Andersson, and for discussions with N. W. Evans, G. W. Gibbons and J. E. Pringle.

APPENDIX A: STATIC DISKS

Some characteristic features of the sources of axisymmetric stationary spacetimes can already be observed in the case of static spacetimes. While in the main text we use the geometric approach [30] to get the stress-energy tensor, here we will directly look at the components of the Einstein equations in Weyl coordinates in which the metric reads [29]

$$ds^2 = -e^{2\nu}dt^2 + e^{2\zeta-2\nu}(d\rho^2 + dz^2) + e^{2\nu}\rho^2 d\phi^2. \tag{A1}$$

Assume we have two solutions $\nu^{\pm}$, $\zeta^{\pm}$ of the field equations

$$\Delta\nu = 0, \tag{A2}$$

$$\zeta_z = 2\rho\nu_\rho\nu_z, \tag{A3}$$

$$\zeta_\rho = \rho(\nu_\rho^2 - \nu_z^2) \tag{A4}$$

in the regions $z > 0$ and $z < 0$ which are continuous across $z = 0$, i.e., $\nu^+(\rho, z = 0) = \nu^-(\rho, z = 0)$ and $\zeta^+(\rho, z = 0) = \zeta^-(\rho, z = 0)$. Hence, the radial partial derivatives of the potentials are also equal along the plane $z = 0$ and Eqs. (A3) and (A4) guarantee that we either have continuity of the normal derivatives of both potentials (and hence no surface source) or the situation is reflection-symmetric when $\nu_z^+(\rho, z = 0) = -\nu_z^-(\rho, z = 0)$ and $\zeta_z^+(\rho, z = 0) = -\nu_z^-(\rho, z = 0)$. Then the Einstein equations have two nonvanishing components which, under these assumptions, can be written as follows:

$$G_{tt} = 2e^{4\nu-2\zeta}(\rho\nu_\rho - 1)\Delta\nu = 8\pi S_{tt}\delta(z), \tag{A5}$$

$$G_{\phi\phi} = -2e^{-2\zeta}\rho^3\nu_\rho\Delta\nu = 8\pi S_{\phi\phi}\delta(z). \tag{A6}$$

Here $\Delta\nu = 2\nu_z^+|_{z=0}\delta(z)$, so these equations directly describe how the discontinuity of the normal derivatives generates the components of the surface stress-energy tensor S_{tt} and $S_{\phi\phi}$. The remaining components of the Einstein tensor contain only the first derivatives of the potentials and vanish identically.

The reflection symmetry across $z=0$ can easily be achieved by using $\nu^-(\rho,z)=\nu^+(\rho,-z)$. Thus any solution of the Poisson equation $\Delta\nu=\lambda(\rho,z)$ for any λ such that $\lambda(\rho,z>0)=0$ can be used to generate a vacuum static spacetime with an axisymmetric disk source.

Therefore, we conclude that (i) gluing along the "planes" with the Weyl coordinate $z=\text{const}$ yields no radial stresses, (ii) the model of the surface stress-energy tensor has to provide a mechanism that generates $S_{\phi\phi}$ as a consequence of which the disk matter resists the radial acceleration, and (iii) while in the Newtonian limit we get $\Delta\nu=-4\pi\sigma\delta(z)$, (iv) in the strong field the sign of $-\Delta\nu$ and that of the energy density may not coincide [e.g., due to the term $\rho\nu_\rho-1$ in Eq. (A5)] and thus the source cannot be made from realistic matter.

APPENDIX B: TOTAL MASS AND ANGULAR MOMENTUM

The method of the construction of the disk sources we employ guarantees that the values of the total mass and angular momentum given by the asymptotic behavior of the metric are equal to those of the original spacetimes. Using the Komar approach, the stationary spacetimes with Killing vectors corresponding to the time and axial symmetries enable us to write these quantities as integrals of surface densities over the disk.

The mass M defined by the asymptotic behavior of the metric can be expressed as an integral of the stress-energy tensor components over the spacelike hypersurface Σ surrounding the regions of nonvanishing $T_{\mu\nu}$.

The Komar mass integral (see e.g., Ref. [33]),

$$M=-\frac{1}{8\pi}\int_{\partial\Sigma}\nabla^\mu\xi^\nu d\Sigma_{\mu\nu}, \tag{B1}$$

can be evaluated over any two-dimensional boundary of the spacelike hypersurface Σ surrounding all sources $T^{\mu\nu}\neq 0$ so for disk-like sources we can integrate over the area of the disk. For an antisymmetric tensor $A^{\mu\nu}$ the integration over the upper part of the disk takes the form

$$\int A^{\mu\nu}d\Sigma_{\mu\nu}=2\int(A^{t\rho}z_{,s}-A^{tz}\rho_{,s})\sqrt{-g}dsd\phi. \tag{B2}$$

Since $A^{t\rho}z_{,s}-A^{tz}\rho_{,s}=A^{\mu\nu}\delta^{(t)}_\mu n_\nu e^{2\nu-2\zeta}\lambda^{-1}$, the timelike Killing vector $\xi^\mu=e^\nu e^\mu_{(t)}$ and $\delta^{(t)}_\mu=-e^{-\nu}(e_{\mu(t)}+\rho^{-1}Ae^{2\nu}e_{\mu(\phi)})$, we can, regarding Eq. (9), express the Komar mass (B1) in terms of the discontinuity of the first derivatives (denoted again as $[\ldots]$)

$$M_D=-\frac{1}{4\pi}\int_D\left([K_{(t)(t)}]+\frac{Ae^{2\nu}}{\rho}[K_{(t)(\phi)}]\right)dS, \tag{B3}$$

where $dS=\rho\lambda^{-1}(s)dsd\phi$ is an area element inside the disk. This then yields Eq. (18), and if disks without the radial pressure are considered and the line element (1) giving $g=-\rho^2g_{\rho\rho}g_{zz}$ is used, we get

$$M_D=\int_D(S^\phi_\phi-S^t_t)\sqrt{g_{\rho\rho}}2\pi\rho\,d\rho. \tag{B4}$$

Since we use the circumferential radius as a common coordinate to compare the mass density curves of the disks with different parameters and with different intrinsic geometries, we transform this integral into the form (40).

The total angular momentum in an axisymmetric stationary spacetime can be defined by the expression [33]

$$J=\frac{1}{16\pi}\int_{\partial\Sigma}\nabla^\mu\eta^\nu d\Sigma_{\mu\nu}, \tag{B5}$$

where η^ν is the axial Killing vector field. Again, these integrals can be rewritten as integrals over the surface of the disk

$$J_D=-\frac{1}{8\pi}\int_D\Big\{[K_{(t)(\phi)}](1+\rho^{-2}A^2e^{4\nu}) +\rho^{-1}Ae^{2\nu}([K_{(t)(t)}]+[K_{(\phi)(\phi)}])\Big\}\rho dS. \tag{B6}$$

In terms of the metric potentials this turns into Eq. (19) and for disks without radial pressure we get Eq. (41). Apart from indicating the properties of the disk, the formulas for M_D and J_D can also be used as independent checks of the code that evaluates S_{ab}, since the total spacetime mass and angular momentum are known.

[1] J. Bičák, D. Lynden-Bell, and C. Pichon, Relativistic discs and flat galaxy models, Mon. Not. R. Astron. Soc. **265**, 126 (1993).

[2] N. W. Evans and P. T. de Zeeuw, Potential-density pairs for flat galaxies, Mon. Not. R. Astron. Soc. **257**, 152 (1992).

[3] J. Bičák, D. Lynden-Bell, and J. Katz, Relativistic disks as sources of static vacuum spacetimes, Phys. Rev. D **47**, 4334 (1993).

[4] G. Neugebauer and R. Meinel, General Relativistic Gravitational Field of a Rigidly Rotating Disk of Dust:

Solution in Terms of Ultraelliptic Functions, Phys. Rev. Lett. **75**, 3046 (1995).
[5] G. Neugebauer, A. Kleinwaechter, and R. Meinel, Relativistically rotating dust, Helv. Phys. Acta **69**, 472 (1996).
[6] C. Klein and O. Richter, Exact Relativistic Gravitational Field of a Stationary Counterrotating Dust Disk, Phys. Rev. Lett. **83**, 2884 (1999).
[7] J. Frauendiener and C. Klein, Exact relativistic treatment of stationary counterrotating dust disks: Physical properties, Phys. Rev. D **63**, 084025 (2001).
[8] T. Morgan and L. Morgan, The gravitational field of a disk, Phys. Rev. **183**, 1097 (1969).
[9] J. Bičák and T. Ledvinka, Relativistic Disks as Sources of the Kerr Metric, Phys. Rev. Lett. **71**, 1669 (1993).
[10] C. Pichon and D. Lynden-Bell, New sources for Kerr and other metrics: Rotating relativistic discs with pressure support, Mon. Not. R. Astron. Soc. **280**, 1007 (1996).
[11] D. Vogt and P. S. Letelier, Relativistic models of galaxies, Mon. Not. R. Astron. Soc. **363**, 268 (2005).
[12] G. A. González and A. C. Gutiérrez-Piñeres, Stationary axially symmetric relativistic thin discs with nonzero radial pressure, Classical Quantum Gravity **29**, 135001 (2012).
[13] A. C. Gutiérrez-Piñeres, G. A. González, and H. Quevedo, Conformastatic disk-haloes in Einstein-Maxwell gravity, Phys. Rev. D **87**, 044010 (2013).
[14] T. Ledvinka, M. Žofka, and J. Bičák, Relativistic disks as sources of Kerr-Newman fields, in *Proceedings of MG8 Meeting, Jerusalem*, edited by T. Piran and R. Ruffini (World Scientific, Singapore, 1999), p. 339.
[15] C. Klein, On explicit solutions to the stationary axisymmetric Einstein-Maxwell equations describing dust disks, Ann. Phys. (Berlin) **12**, 599 (2003).
[16] J. P. S. Lemos and P. S. Letelier, Exact general relativistic thin disks around black holes, Phys. Rev. D **49**, 5135 (1994).
[17] D. Vogt and P. S. Letelier, General relativistic model for the gravitational field of active galactic nuclei surrounded by a disk, Phys. Rev. D **71**, 044009 (2005).
[18] V. Karas, J.-M. Huré, and O. Semerák, Topical review: Gravitating discs around black holes, Classical Quantum Gravity **21**, R1 (2004).
[19] P. Suková and O. Semerák, Free motion around black holes with discs or rings: Between integrability and chaos–III, Mon. Not. R. Astron. Soc. **436**, 978 (2013).
[20] A. Tomimatsu and H. Sato, New series of exact solutions for gravitational fields of spinning masses, Prog. Theor. Phys. **50**, 95 (1973).
[21] A. Tomimatsu and H. Sato, Event horizon of the Tomimatsu-Sato metrics, Lett. Nuovo Cimento **8**, 740 (1973).
[22] G. W. Gibbons and R. A. Russell-Clark, Note on the Sato-Tomimatsu Solution of Einstein's Equations, Phys. Rev. Lett. **30**, 398 (1973).
[23] H. Kodama and W. Hikida, Global structure of the Zipoy Voorhees Weyl spacetime and the $\delta = 2$ Tomimatsu Sato spacetime, Classical Quantum Gravity **20**, 5121 (2003).
[24] V. C. Rubin, J. A. Graham, and J. D. P. Kenney, Cospatial counterrotating stellar disks in the Virgo E7/S0 galaxy NGC 4550, Astrophys. J. Lett. **394**, L9 (1992).
[25] E. Iodice and E. M. Corsini, Multi-Spin Galaxies, Astronomical Society of the Pacific Conference Series Vol. **486** (ASPSC, San Francisco, 2014).
[26] R. Bassett, K. Bekki, L. Cortese, and W. Couch, The formation of S0 galaxies with counter-rotating neutral and molecular hydrogen, Mon. Not. R. Astron. Soc. **471**, 1892 (2017).
[27] S. Dyda, R. V. E. Lovelace, G. V. Ustyugova, M. M. Romanova, and A. V. Koldoba, Counter-rotating accretion discs, Mon. Not. R. Astron. Soc. **446**, 613 (2015).
[28] A. R. King, J. E. Pringle, and J. A. Hofmann, The evolution of black hole mass and spin in active galactic nuclei, Mon. Not. R. Astron. Soc. **385**, 1621 (2008).
[29] H. Stephani, D. Kramer, M. MacCallum, C. Hoenselaers, and E. Herlt, *Exact Solutions of Einstein's Field Equations* (Cambridge University Press, Cambridge, England, 2009).
[30] W. Israel, Singular hypersurfaces and thin shells in general relativity, Il Nuovo Cimento B **44**, 1 (1966).
[31] C. Barrabès and W. Israel, Thin shells in general relativity and cosmology: The lightlike limit, Phys. Rev. D **43**, 1129 (1991).
[32] K. Kuchař, Charged shells in general relativity and their gravitational collapse, Czech. J. Phys. **18**, 435 (1968).
[33] R. M. Wald, *General Relativity* (University of Chicago Press, Chicago, 1984).
[34] R. H. Boyer and R. W. Lindquist, Maximal analytic extension of the Kerr metric, J. Math. Phys. (N.Y.) **8**, 265 (1967).
[35] C. Hoenselaers, Weyl conform tensor of the Tomimatsu-Sato $\delta = 3$ metric, Gen. Relativ. Gravit. **11**, 325 (1979).
[36] A. Tomimatsu and H. Sato, New Exact Solution for the Gravitational Field of a Spinning Mass, Phys. Rev. Lett. **29**, 1344 (1972).
[37] B. Carter, Global structure of the Kerr family of gravitational fields, Phys. Rev. **174**, 1559 (1968).
[38] A. S. Tahvildar-Zadeh, On a zero-gravity limit of the Kerr-Newman spacetimes and their electromagnetic fields, J. Math. Phys. (N.Y.) **56**, 042501 (2015).
[39] O. Brauer, H. A. Camargo, and M. Socolovsky, Newman-Janis algorithm revisited, Int. J. Theor. Phys. **54**, 302 (2015).
[40] J. Bičák, O. Semerák, and P. Hadrava, Collimation effects of the Kerr field, Mon. Not. R. Astron. Soc. **263**, 545 (1993).
[41] G. Neugebauer and R. Meinel, The Einsteinian gravitational field of the rigidly rotating disk of dust, Astrophys. J. Lett. **414**, L97 (1993).
[42] Z. Perjés, Factor structure of the Tomimatsu-Sato metrics, J. Math. Phys. (N.Y.) **30**, 2197 (1989).